Hydrological Impacts of Climate Change On Lake Tana's Water Balance

ZEMEDE MULUSHEWA NIGATU

March. 2013

SUPERVISORS:
Dr. ing. T.H.M. (Tom) Rientjes
Dr. ir. C. (Christiaan) van der Tol

Hydrological Impacts of Climate Change On Lake Tana's Water Balance

ZEMEDE MULUSHEWA NIGATU
Enschede, The Netherlands, [March, 2013]

Thesis submitted to the Faculty of Geo-Information Science and Earth Observation of the University of Twente in partial fulfilment of the requirements for the degree of Master of Science in Geo-information Science and Earth Observation.
Specialization: Water resource and Environmental Management

SUPERVISORS:
Dr. ing. T.H.M. (Tom) Rientjes
Dr. ir. C. (Christiaan) van der Tol

THESIS ASSESSMENT BOARD:
Dr. ir. C.M.M. (Chris) Mannaerts (Chair)
Dr. P. Reggiani (External Examiner, Deltares, The Netherlands)
Dr. ing. T.H.M. (Tom) Rientjes
Dr. ir. C. (Christiaan) van der Tol

ABSTRACT

One of the most momentous potential concerns of climate change is to understand changes in hydrological components and subsequent change in lakes water balance. The water balance components such as surface water inflow from gauged and ungauged catchments, over-lake precipitation and evaporation pattern alteration and their impact on Lake Tana water balance is analysed. The main aim of this study is to evaluate the hydrological impacts of climate change on the water balance of Lake Tana in Ethiopia. The Lake Tana is the largest lake in Ethiopia and the third largest in Africa, which is located in Amahara regional state in Ethiopia.

The precipitation, maximum and minimum temperature at Lake Tana catchment level for A2 and B2 scenarios downscaled from HadCM3. This was downscaled using Statistical DownScaling Model (SDSM 4.2). The Regional Climate Model (i.e. CCLM) generates the A1B scenario. The bias correction in the A1B scenario for precipitation, maximum and minimum temperature was done by using Linear-scaling approach, before using it for water balance analysis. This analysis is based on projection of three different scenarios of climate change for future time horizons: 2020s (2010-2039), 2050s (2040-2069) and 2080s (2070-2099). Over-lake evaporation is estimated by Hardgrave's method, over-lake precipitation is computed by inverse distance weighing method and surface inflows are simulated by using HBV model.

The result revealed that the maximum and minimum temperatures increase for all the three scenarios in all future time horizons. However, precipitation does not show a systematic increase or decrease in all future time horizons. The inflows to the lake, over-lake precipitation and evaporation and storage at the lake show an increasing pattern for scenarios A2 and B2. The A1B scenario reveals the decreasing pattern of lake water storage due to decrease of inflows components such over lake precipitation and surface water inflow in all future time horizons. In this scenario, the over-lake evaporation shows increasing pattern for all future time horizons.

Key words: Water Balance, Lake Tana, Climate change, SDSM

ACKNOWLEDGEMENTS

First and Foremost, I would like thank the almighty God for his endless grace and blessings, for answering my prayers, for giving me the strength to accomplish my thesis on despite of my constitution wanting to give up during my MSc study and through my life. Thank you so much dear Lord!

Foremost, I gratefully acknowledge the contribution of my first supervisor, Dr. Ing. T.H.M. Tom Rientjes, whose patient guidance, dedication, and knowledge guided me throughout the thesis work. I would like to extend my acknowledgement to my second supervisor, Dr. Ir. C. Christiaan van der Tol for incredible guidance and reviewing my work. It was a great pleasure to work with them and I have been so lucky to have supervisors who cared so much about my thesis work, and who answered to my requests and queries so punctually.

I would like to express my sincere appreciation to the directorate of ITC for awarding me this opportunity to study for a Master of Science degree. I am also grateful to Netherland Fellowship program (NFP) for their financial support throughout my study.

I would like to thanks also Ethiopian National Meteorological Agency for providing meteorological data, Dr. Solomon S. Demissie for provision of CCLM data from International Water Management Institute (IWMI), HadCM3 center for SDSM model provision for my study.

I thank my fellow collogues for the motivating discussions, for working together without ceasing before the deadlines, and for all the fun we have had during MSc study period.

Lastly but not least, I wish to express my deep appreciation to all friends and family members back at home. Their prayers kept me so encouraged and inspired even at tough time to accomplish my study without ceasing.

Dedicated to the Almighty God,
Creator of Heaven and Earth,
My help in the time of need,
One who is, who was, and who is coming!

TABLE OF CONTENTS

LIST OF FIGURES

LIST OF TABLES

ACRONYMS AND ABREVATIONS

AOGCM	Coupled Atmospheric-Ocean General Circulation Model
A1B	Moderate emission scenario
A2	Medium to high emission scenario
B2	Medium to low emission scenario
CCLM	COSMO-Climate Limited-area Modelling
CICS	Canadian Institute for Climate Studies
COSMO	Consortium for Small scale Modelling
DEM	Digital Elevation Model
ECHAM4	European Center HAMburg 4
ETo	Reference Evapotranspiration
ETp	Potential Evaporation
FAO	Food and Agriculture Organization of the United Nations
FORTRAN	Formula Translation/Translator
HadCM3	Hadley Centre Coupled Model version3
HBV	Hydrologiska Byråns Vattenbalansavdelning (hydrological model)
GCM	General Circulation Model
CGCM2	Second-Generation Coupled Global Climate Model
GCP	Ground Control Point
ILWIS	Integrated Land and Water Information System (software)
IPCC	Intergovernmental Panel on Climate Change
IWMI	International Water Management Institute
MATLAB	Matrix Laboratory
MODIS	Moderate Resolution Imaging Spectroradiometer
NASA	National Aeronautics and Space Administration (USA)
NCEP	National Centre for Environmental Prediction
NMA	National Meteorological Agency (Ethiopia)
PET	Potential Evapotranspiration
PIK	Potsdam Institute for Climate Impact Studies
RCD	Regional Climate Downscaling
RCM	Regional Climate Model
SDSM	Statistical Downscaling Model
SRES	Special Report on Emission Scenarios
SRTM	Shuttle Radar Topographic Mission
SRES	Special Report on Emission Scenario
WMO	World Meteorological Organization

1. INTRODUCTION

1.1. Background

In GWPF (2011), climate change is described as "a change in the state of the climate that can be identified by changes in the mean and/or statistical distribution of weather variables for extended period, typically decades or longer. It has its own key indicators and different causes and effects. It may be due to natural internal processes or external forcing of continual anthropogenic change". Rising of global surface temperature, sea level rises, arctic and land ice decrease, erratic precipitation and increase of CO2 concentration are main indicators of climate change (NASA,2010). Shift in temperature and precipitation patterns affects the hydrology process and availability of water resources. Globally rising temperature and atmospheric circulation patterns likely cause changes in the frequency and seasonality of precipitation and also may result an overall boost on evaporation and precipitation rate.

In many parts of the world climate is both changed and varying. Changes are from humid equatorial to seasonally-arid tropical regimes and varying because climates reveal differing extent of temporal and spatial unevenness (Hulme et al.,2001). Climate change is commonly projected at continental or global scale, the magnitude and type of impact at regional-scale catchments is not investigated in many parts of the world that also includes Lake Tana in Ethiopia (Abdo et al.,2009). Hydrological impacts of climate change on the Lake Tana water balance are not well researched, even though some studies on climate change impacts in the upper Blue Nile have been done (Beyene et al.,2010; Kim et al.,2009). None of these studies focused on hydrological impact of climate change on the water balance of Lake Tana.

Lake Tana occupies a wide depression in the Ethiopian plateau with 3156 km^2 in area. It is the third largest Lake in the Nile Basin and largest lake in Ethiopia. It is approximately 84 km long and 66 km wide. The water balance of the lake accounts all inflows and outflows in a given period. The term inflow refers to lake precipitation and surface runoff from gauged and ungauged catchments into the lake. Outflow refers to evaporation and stream flow through the Blue Nile (Abay) River. Based on Rientjes et al. (2011a) nine gauged and nine ungauged catchments water inflow from gauged catchments 1254mm/year, ungauged catchment 527mm/year and lake areal precipitation 1347mm/year. Outflow by evaporation was estimated 1563 mm/year whereas River outflow was 1480mm/year with a water balance error of 85mm/year. Chebud et al. (2009) described that Lake Tana historical variation level assumed to stem from hydrological alterations within its basin due to reduction in dry season flows attributed to human and climate induced changes.

1.2. Research Problem

One of the most momentous potential concerns of climate change is hydrological components alteration and subsequent changes in lakes water balance. Among the water balance components surface water inflow from ungauged and gauged catchments, over-lake precipitation and evaporation pattern alteration and their impact on Lake Tana water balance is not yet researched well. Therefore, this study investigates the pattern of hydrological alteration and determines pattern of climate change with its impact on the Lake Tana water balance.

General Circulation Model (GCM) outputs are not directly applicable at regional scale due to coarse resolution of the model grid scale. According to Abdo et al. (2009) changes in climate are commonly

projected at continental or global scale, but the magnitude and type of impact at regional-scale catchments is not investigated in many parts of the world that also includes Lake Tana in Ethiopia. Kim et al. (2009) and Beyene et al. (2010) studied climate change impact in upper blue Nile by using direct GCM outputs that has high uncertainty but did not focus on downscaling at Lake Tana level. In this study A2 and B2 scenario are downscaled by SDSM and A1B scenario of RCM output is used to evaluate hydrological impacts on Lake Tana water balance.

1.3. Research Objective

1.3.1. General Objective

The general objective of this study is to evaluate hydrological impacts of climate change on the water balance components of Lake Tana in Ethiopia.

1.3.2. Specific Objectives

The specific objectives of this study are:

1. To identify possible changes of lake Tana water balance due to climate change in the 21st century
2. To downscale the A2 and B2 scenarios from the HadCM3 using meteorological station data around Lake Tana
3. To compare the RCM & SDSM output (i.e. precipitation, maximum and minimum temperature) with observed patterns from meteorological station records
4. To evaluate the future change pattern of RCM outputs and SDSM downscaled maximum and minimum temperature , precipitation and estimated evaporation

1.4. Research Questions

In order to meet the research objectives, the research questions for this study are:

1. What is the general pattern of ground based measured precipitation, potential evaporation, maximum and minimum temperature for the baseline period?
2. What is the general pattern of past and future RCM and SDSM output parameters mentioned at question 1 of Lake Tana and its catchments?
3. How do these patterns affect the water balance components of Lake Tana?

1.5. Assumptions and Limitation of the study

In this study the current land cover condition and lake-outflow through Blue Nile River is assumed to remain the same for the future period. As such it is assumed that land cover and long year mean annual outflows from the lake will not change. Ground water flow towards and from the lake is assumed to be negligible as suggested by (Chebud et al.,2009).

In addition to the assumptions made, this study has been done within a framework of few limitations. Among these climate emission scenarios and the SDSM model used to downscale GCM scenarios that has their own uncertainty that may produce error on the lake water balance. Data collected from meteorological stations also has its own draw back due to missing, outlier and observation error as presented in Appendix A.

1.6. Thesis Outline

This thesis work is organized in six chapters as follows. Chapter one introduces the study with its objective, relevance and research questions. Chapter two deals with the state-of-the-art review related to the study. Chapter three gives a brief description of the study area. Chapter four deals with the material and methodology adopted for the study. In chapter five results are presented and discussed. Finally chapter six ends with the general conclusions and recommendations of the study as well as propositions for future research.

2. LITERATURE REVIEW

2.1. Hydrological impact of Climate change

All across the world people are taking action because climate change has serious impacts, locally and globally. Centres for climate change data (http://www.world.org/weo/climate) and for research (http://www.eecg.utoronto.ca/~prall/climate/univ_climate_sites.html) are forced to give attention for climate change study and data processing or dissemination. Scientists from the International Panel on Climate Change (IPCC) predicted that warming of oceans and melting of glaciers and thus could cause global sea levels to rise of 17-58centimetres by the year 2100. As such, densely inhabited coastal communities and infrastructure would be affected by enhanced flooding, drought and high sea level.

Hydrological climate change impact assessment involves recognizing three key aspects of uncertainty (Abdo et al.,2009). These are: 1) GCMs linked uncertainties; 2) downscaling methods that are uncertain in the representation of climatology at regional and local scales; and 3) parameter uncertainties and structural deficiencies in the hydrological models. Uncertainties in climate scenarios and GCM outputs, however, may be considered much larger although the GCMs ability to reproduce the current climate has increased over the past decade.

2.2. Global Circulation Models (GCMs)

GCM stands for general circulation model representing model representing physical processes interactions of the atmosphere-ocean-cryosphere-land surface. GCMs are the most multifaceted tools currently available for simulating the response of the global climate system. Many GCMs illustrate global climate in 3D-grid with horizontal resolution from 2.5° latitudes by 3.75° longitudes for atmospheric component to 1.25° Latitudes by 1.25° longitudes for oceanic component (Gordon et al.,2000). This resolution is coarse relative to the scale of exposure for applicability in impact assessments criteria (see section 2.5) and it causes uncertainties. These uncertainties can be manifested in GCM-based simulations of future climate and various feedbacks. Among many, some feedbacks are water vapoure and warming, ocean circulation and ice/snow albedo, cloud and radiation. GCMs may simulate quite different responses by the same forcing due to differences in feedbacks and process models.

2.3. The climatological baseline

World Meteorological Organization (WMO) defines climatological baseline as a thirty-year "normal" period that can provides a standard reference for impact studies. Commonly the baseline is used as the reference period from which the modelled future change in climate is calculated (Houghton et al.,2001). It is important to make basis for assessing future impacts of climate change to acquire a quantitative description of the changes to be expected. According to IPCC (1994) possible criteria for selecting the baseline period are representativeness for the present-day, recent average climate and sufficient duration to encompass a range of climatic variations. Carter (2007) listed alternative sources of baseline climatological data for impact assessments, these sources are National Meteorological Agencies archives, supranational and global data sets, outputs of climate models and weather generators. For this study Ethiopian National Meteorological Agency (NMA) archive data is used as baseline data for the period of 1980-2010.

2.4. Emission Scenarios

IPCC (2000) defines emission scenario as “images of the future or alternative futures .They are neither forecasts nor predictions; rather all scenarios are one alternative image of how the future might reveal”.

A climate scenario must be representative, consistent and be a reasonable projection of possible future climates. It is not a forecast or prediction but it is an alternative image of how the future can be explained and its raw material is projected (IPCC,2012). It should fulfil five criteria to be used for impact assessments and policy makers. According to IPCC (2012) report, these criteria are consistency with global projection, physical plausibility, applicability for impact assessments, representativeness and accessibility.

Consistency with global projections indicates unfailing with broad range of global warming projection based on increased concentration of greenhouse gases. This range is 1.4°C to 5.8°C by 2100, or 1.5°C to 4.5˚C where atmospheric CO_2 concentrations amplify. Physical plausibility means they should respect the basic laws of physics (i.e. the laws that we understand and can apply at global scale). Therefore, changes in a certain area should be physically consistent with those in another region and globally. Applicability in impact assessments shows availability of spatial-temporal scale climate variables changes that enables for impact assessment. Representative means that a scenario should be able to represent the future regional climate change potential range. Only in this way, a realistic range of possible impacts can be estimated. Accessibility means straightforward ability to interpret and apply for impact assessment. The term projection can be regarded as any description of the future and the pathway leading to it or refers to model-derived estimates of future climate (Moss et al.,2010).

Based on these criteria the A2 (medium–high), B2 (medium-low) A1B (balanced) emission scenarios are selected for this study. These scenarios are widely used in most GCM as well as RCM models. According to (IPCC,2007) "A2 scenario represents a very heterogeneous world with continuously increasing global population(not higher than A2) and regionally oriented economic growth that is more fragmented and slower than in different storyline. B2 scenario refers a heterogeneous world in which the emphasis is on local solutions to social, environmental and economic sustainability. A1B scenario is emission scenario with balanced dependence on all energy sources". For detail explanation A2, B2 and A1B scenarios see Appendix C.

Some of previous studies conducted in the Upper Blue Nile based on A2, B2 and A1B scenarios are summarized as follows. Soliman et al. (2009) assessed the future climate change for the Blue Nile Basin by using A1B emissions scenario and the result indicates that the changes in future rainfall might vary over different areas of the Upper Blue Nile catchment in Ethiopia. (Elshamy et al.,2009) studied impacts of climate change on the Nile Flows at Dongola using statistical downscaled GCM (i.e. CGCM2, ECHAM4, and HadCM3) A2 and B2 scenarios; the study result indicates that the range of differences between the scenarios is model dependent and time dependent.

Incremental scenario refers to arbitrary amount changes of a particular climate element. They are used to evaluate system sensitivity before the application of a more credible model based scenario. According to Carter (2007), adjustments of baseline temperature by +1, +2, +3, +4ºC and precipitation by ±5%, ±10%, ±15%, ±20 % could represent various magnitude of future change. However, such scenarios do not necessarily present a set of changes that are physically realistic; they provide information on an ordered range of climate changes for direct intercomparison of results.

2.5. Climate data downscaling

Downscaling climate data is an approach for generating locally applicable data from Global Circulation Models. The ultimate goal of downscaling is to connect global scale experiments / predictions and regional dynamics to produce regionally specific simulations (Climate-decisions.org,2008). Downscaling is commonly done either by using Regional Climate Downscaling (RCD) or Statistical DownScaling

Methods (SDSM). RCD has been increasingly used to address a variety of climate-change issues and have by now become an important method in climate change research (WMO,2008).

2.5.1. Regional Climate Models (RCMs)

Regional climate models (RCMs) are nested within global climate models (GCMs) (Figure 1). They provide a dynamically consistent way to downscale the coarse GCM results to local detail for a limited area of interest. The use of RCMs for climate application was initiated by (Dickinson et al.,1989; Giorgi et al.,1990) and has all-embracing range in climate studies from natural to human-induced climate change studies. The RCM technique comprises of using initial, surface boundary and time-dependent lateral meteorological conditions to drive high-resolution RCMs.

RCM can provide high spatial resolution (up to 10 to 20 km or less) and multi-decadal simulations climate data and are capable of describing climate feedback mechanisms acting at the regional scale. The main theoretical limitations of RCM technique are: systematic errors (Berg et al.,2012) in the driving fields provided by global models; lack of two-way interactions between regional and global climate; computational demand; need of careful co-ordination between global and regional modellers to perform RCM experiments Environment Canada (2012).

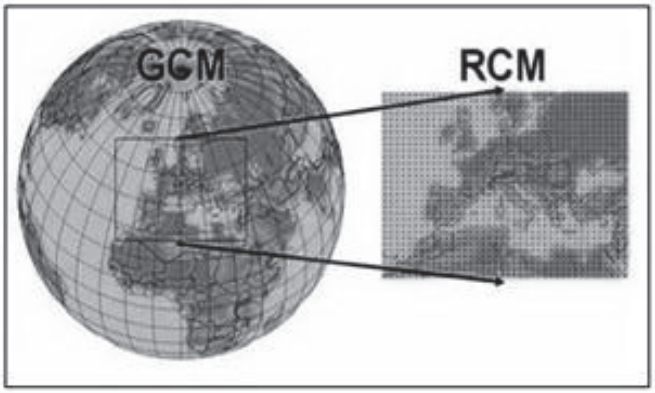

Figure 1: Regional Climate Model nesting approach (WMO,2008)

2.5.2. Statistical DownScaling Model (SDSM)

Statistical Downscaling Model (SDSM) is used to downscale from coarse-resolution climate model (i.e. GCM) simulations to produce high spatial-resolution climate data. Whenever climate change impact study requires small-scale climate scenarios, SDSM provides quality observational and projected data of daily GCM outputs for specific location. A range of statistical downscaling models were used in climate change studies (Huang et al.,2012; Teutschbein et al.,2011) and techniques applied were weather typing, stochastic weather generator and regressions. Some disadvantages and advantages of SDSM in comparison with RCM method is described in Table 1.

Table 1: Comparison of the advantages and disadvantages between RCM and SDSM (This study)

RCM	SDSM
Uses finer resolution RCM with horizontal resolution 20-50km	Uses courser resolution GCM output
Not limited by the assumption of temporal stationary empirical relations	Limited by the assumption of temporal stationary empirical relations
Physically based and reasonably convertible from current to the future climate	Statistically based
Can resolve small scale atmospheric features (e.g. orographic precipitation)	Empirically-based techniques cannot account for possible systematic changes in regional forcing conditions or feedback processes
Requires considerable computing resource and expensive to run	Computationally inexpensive, easily be applied to output from different GCM experiments
Couple atmospheric models with other climate process models (hydrology, land-biosphere...)	Cannot manage remote regions or regions with complex topography

2.6. Water Balance of Lake Tana

2.6.1. Lake Water Balance

The water balance of a lake is accounting for all water entering and leaving the lake for a given period. The term entering (inflow) refers to ground water leakage, lake precipitation, and surface runoff from gauged and ungauged catchments. Outflow refers to evaporation and flow through channels. In case of Lake Tana the most dominant water balance components are evaporation, precipitation, surface runoff into the lake from 13 gauged and ungauged catchments and outflow through the Blue Nile River (Rientjes et al.,2011b).

2.6.2. HBV model

HBV-96 model is a conceptual model with applications range from lumped model to semi distributed model domains. Detail description of this model adopted from (SMHI,2006) is presented in section 4.6. Originally, it was established for runoff simulation and hydrological prediction but today it is used for water balance studies, runoff forecasting, dam safety, for assessments and simulation of climate change impacts (Seibert et al.,2002). To simulate surface runoff from gauged and ungauged catchments based on the objective of the study and available data, the HBV model is selected for this study.

Some of the previous studies on climate change that used the HBV model at upper Blue Nile are presented as follows. Abdo et al. (2009) used HBV model to assess impact of climate change on the hydrology of Gilgel Abay catchment in Lake Tana basin, Ethiopia. Bekele (2009) evaluated impact of climate change on Upper Blue Nile Basin Reservoirs (Case Study on Gilgel Abay Reservoir, Ethiopia) by using HBV model.

2.6.3. Over Lake Evaporation

Lake water loss due to evaporation is a large component of the lake's water balance. Accurate and reliable estimation of evaporation depends on extensive data availability. The exact types of data required to estimate evaporation vary considerably and depend on the method used. In fact, research done by Kibret (2009) shows that open water evaporation estimation by satellite remote sensing was better than ground measurements.

Carrillo et al. (2008) compared evaporation estimation methods such as Penman, Hargreaves and Penman-Monteith by using in situ measured weather data and remote sensing data. Among these the standard Penman-Monteith method is recommended by FAO (2012) was combined with the remote sensing techniques gave best result. Albedo from satellite images served as input to the equation and used to calculate the actual evaporation at daily base.

For estimation of lake evaporation the Penman-combination equation (Maidment,2010) uses standard climatological records of daily sunshine hours, temperature, humidity and wind speed as basic inputs. Daily meteorological data should be from stations which are around or with in the study area. Energy balance is combined with a water vapour transfer in Penman-combination for open water evaporation. Detail explanations and the calculation procedure with equations used are presented in section 4.5.2.

2.6.4. Reference Evapotranspiration from catchments

The FAO Penman-Monteith equation comprises all parameters that govern energy exchange and corresponding evapotranspiration from uniform regions of crops. Alternative to the FAO Penman-Monteith equation, the Hardgrave's equation based method is commonly used. Therefore, catchments evapotranspiration can be calculated by Hargreaves's equation and according Hargreaves et al. (1982) it is a temperature based method which has a link to solar radiation (see detail description in section 4.5.3). It often used as a representative expression for potential evapotranspiration.

2.7. Over Lake Rainfall

So far, few studies were conducted to estimate over-lake rainfall to the Lake Tana. Most of these studies were done based on commonly used methods such as Thiessen polygon method, inverse distance weighing method and satellite/remote sensing based methods. Rainfall estimation at daily time series over Lake Tana was done by (Rientjes et al.,2011b) through inverse distance weighted interpolation based on Bahir Dar, Chawhit, Zege, Deke Estifanos and Delgi stations (see Figure 2) for the period 1992–2003. Result of that study indicated that over-lake rainfall of Lake Tana is 1,290 mm/year.

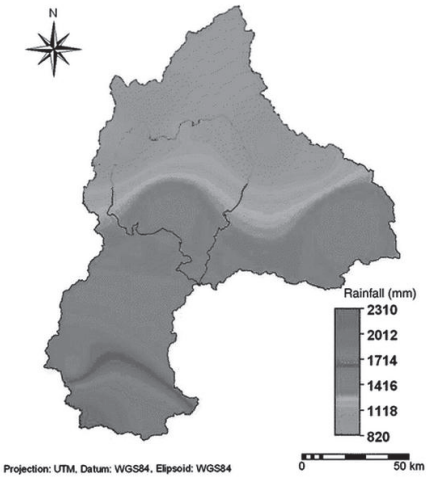

Figure 2: Annual average rainfall (mm) distribution for the period of 1994–2003 in Lake Tana basin (Rientjes et al.,2011b)

3. STUDY AREA AND MATERIALS

3.1. Study Area description

Lake Tana inhabits a wide depression in the Northern part of Ethiopian plateau with approximately 3156 km2 area. Lake Tana with its surrounding catchments covers area bounded 11.50°N to 12.30°N and 36.80°E to 37.80°E (see Figure 3). The lake is the largest lake in Ethiopia and the third largest in the Nile basin with length of 84km and width of 66 km. The lake is situated at nearly 1800 meter elevation in the northern highlands. Numerous seasonal streams feed the lake with four perennial rivers and it depends heavily on the local climate.

According to (Setegn et al.,2010), estimated mean annual precipitation of Lake Tana basin ranges from 1,200 to 1,600 mm and annual mean actual evapotranspiration of the catchments is 773 mm and catchment area water yield is 392 mm for the period of 1961-2000.

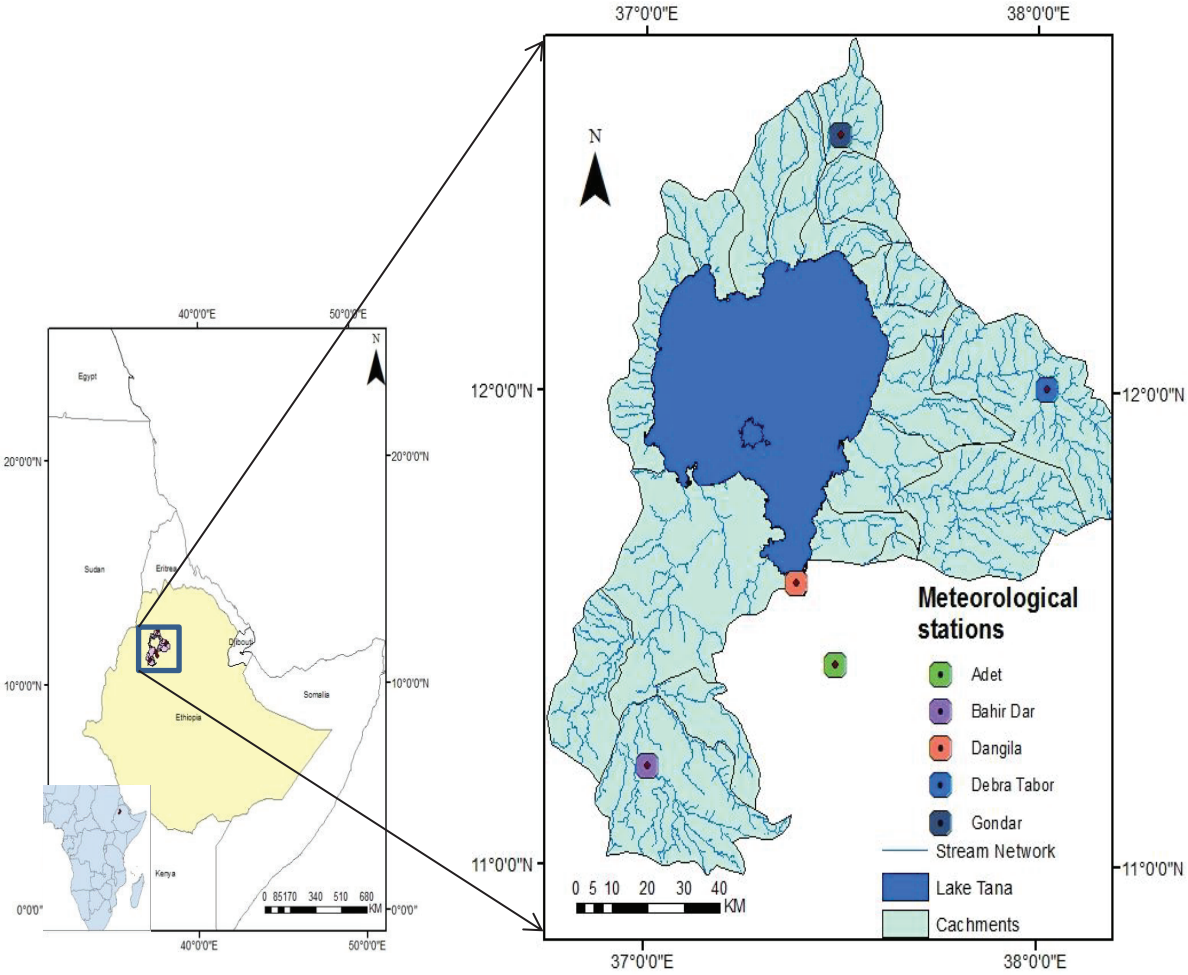

Figure 3: Location of the study area

3.2. Meteorological data

Data of meteorological stations around Lake Tana were collected from Addis Ababa Head office and Bahir Dar branch office of Ethiopian National Meteorology Agency (NMA). According to WMO standard, six principal (see Table 3), six 3rd class and one 4th class weather station are available (see Table 2). A first class (principal) station measures all meteorological variables (i.e. rainfall, maximum and minimum temperature, relative humidity, and wind speed and sunshine hour data), a 3rd class station measures rainfall, maximum and minimum temperature and 4th class station records only rainfall data. These stations have more than 30 years' time series daily data. Not all meteorological and hydrological data should be less than 30years according to WMO standard for climate change studies. Climate scenario data was downscaled by SDSM method and RCM output data collected from International Water Management Institute (IWMI) Addis Ababa.

Table 2: List of meteorological stations, latitude, and longitude and year establishment

Stations	Latitude (°N)	Longitude (°E)	class	Established Year
Gondar	12.52	37.43	1st	1952
Aykel	12.93	37.06	1st	1960
Shahura	11.93	36.87	1st	1997
Bahir Dar	11.52	37.30	1st	1961
Debra Tabor	11.85	38.01	1st	1952
Adet	11.27	37.49	1st	1950
Dangila	11.02	36.72	1st	Not known
Gorgora	12.29	37.29	3rd	1972
Addis Zemene	12.07	37.52	3rd	1974
Deka Estifanos	11.90	37.29	3rd	1960
Zege	11.71	37.32	3rd	1974
Woreta	11.92	37.70	3rd	1969
Enfranz	12.26	37.63	3rd	1977
Delgi	12.19	37.27	4th	1974

(Remark: NA indicates data not available)

Table 3: Meteorological stations used for SDSM downscaling and RCM GCP

	Evaporation/ET		Precipitation			
Stations	Lake	Catchment	Lake	Catchment	SDSM	RCM GCP
Gondar	√	√	√	√	√	√
Bahir Dar	√	√	√	√	√	√
Debra Tabor	√	√	√	√	√	√
Adet	√	√	√	√	√	√
Dangila	√	√	√	√	√	√

Where: ET is evapotranspiration and GCP is ground control point

The Lake Tana basin climate ranges from semi-arid to humid. The main rainy season is called "kiremt" (local name of summer) which occurs June to September and a dry season is known as "bega" (local name of winter) that extends from October to February. The highest peak of rainfall occurs at the month of July. For the period of (1981-2010) mean annual precipitation, mean daily maximum and minimum temperature of study area is presented in Table 4 below.

Table 4: Mean annual precipitation; mean daily maximum and minimum temperatures (1981-2010)

Stations	Tmax(°C)	Tmax(°C)	Precipitation(mm/year)	ETo (mm/year)
Adet	26.1	10.8	1252	-
Bahir Dar	26.8	11.8	1430	2176
Dabra Tabor	21.8	9.5	1462	1790
Dangila	25.3	9.8	1495	-
Gondar	26.7	13.3	1092	2125

3.3. Evapotranspiration of Lake Tana basin

Daily records of relative humidity, wind speed, sunshine hours, maximum and minimum temperature from Bahir Dar, Debre Tabor and Gondar stations were used for the period of 1981-2010. Table 4 shows the mean annual reference evapotranspiration (ETo) estimated by Hargreaves method. ETo for the period of 1981-2010 is 2125mm, 2176mm and 1790 mm at Gondar, Bahir Dar and Debra Tabor stations respectively. In general, reference evapotranspiration showed an overall increase with increase of time. For 30-year period (1981-2010), annual mean and respective year reference evapotranspiration is higher at Bahir Dar and lowest at Debre Tabor stations (see Table 4). Potential evapotranspiration (ETp) (i.e. estimated by Penman combination method) at Bahir Dar and Gondar stations is relatively lower than reference evapotranspiration estimated by Hargreaves method (see Figure 4).

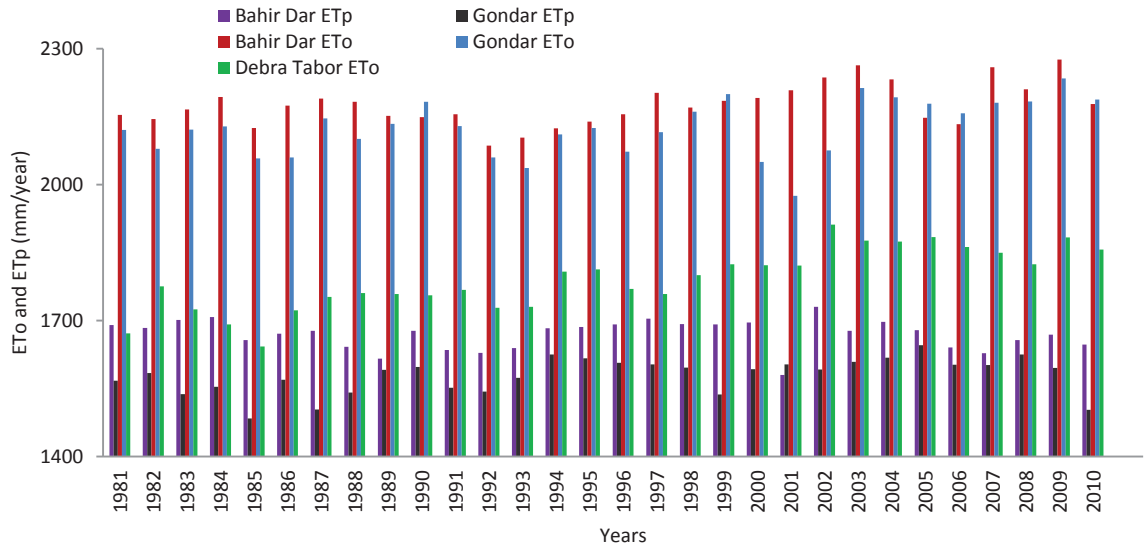

Figure 4: Evaporation (ETp) and Evapotranspiration (ETo) of Lake Tana basin

Figure 4 shows evapotranspiration estimates by Hardgrave's and Penman-Monteith combination method of Lake Tana basin that exhibits both spatial and temporal variability. Temporal variability described by high inter-annual variability with highest record at 2275mm/year in 2009 and lowest record at 1642mm/year in 1985. The highest record at Bahir Dar station that found at southern part of the lake and lowest record at Dabra Tabor station that is located at western part of the lake shows the spatial variation of evapotranspiration at Lake Tana basin.

3.4. Land cover

Based on ITC archive (i.e. previous MSc thesis work data), land cover of Lake Tana basin is classified in to five major parts (see Figure 5). These are cultivated, water body, urban area, forest and grassland. Cultivated area covers approximately 76%, water body comprise 20%, and the urban, forest and grassland covers 4%. This indicates that forest cover the lowest percentage and most of the lake catchments were covered by cultivated land.

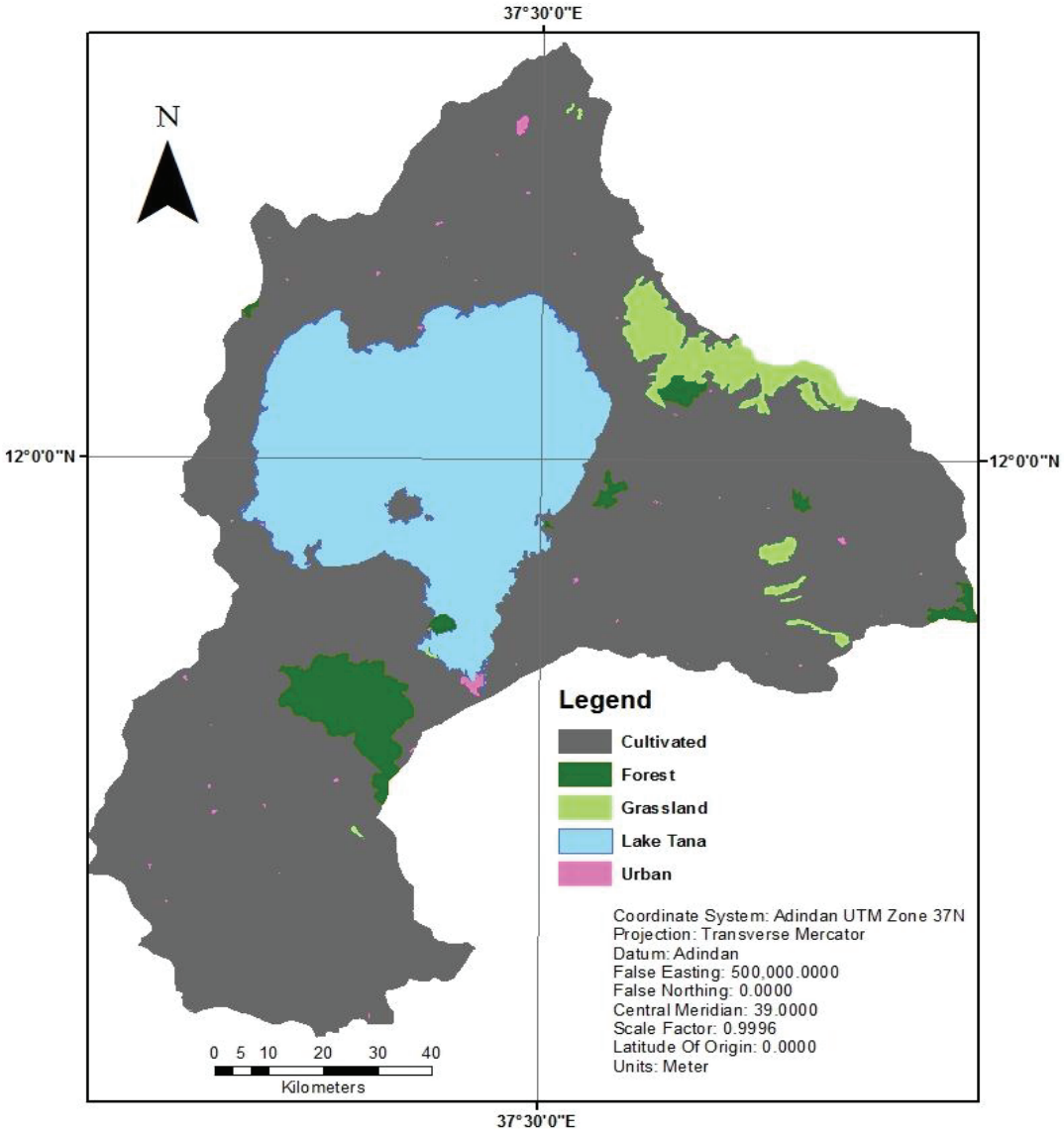

Figure 5: Land cover of study area

3.5. Gauged and ungauged Catchments

A DEM (Digital Elevation Model) of 90m resolution is downloaded from Shuttle Radar Topography Mission (SRTM-version 4) by using GEONETCast ISO toolbox. GEONETCast ISO Toolbox is a plug-in of ILWIS software that offers a set of utilities that assist easy import of various satellite and environmental products that were disseminated via GEONETCast.

The catchments are delineated by using the hydro-processing tool in ILWIS and Arc-GIS software and detailed procedures are described in Appendix D. During delineation the same resolution DEM and

similar delineation approach of previous study of (Perera,2009; Wale,2008) are used. Consequently, the delineation result of previous and current study is more or less the same. Nineteen catchments are extracted (see Figure 6) and among these nine are gauged and the rest ten are ungauged. For all gauged catchments HBV model parameters are calibrated by (Perera,2009) and are used for this study.

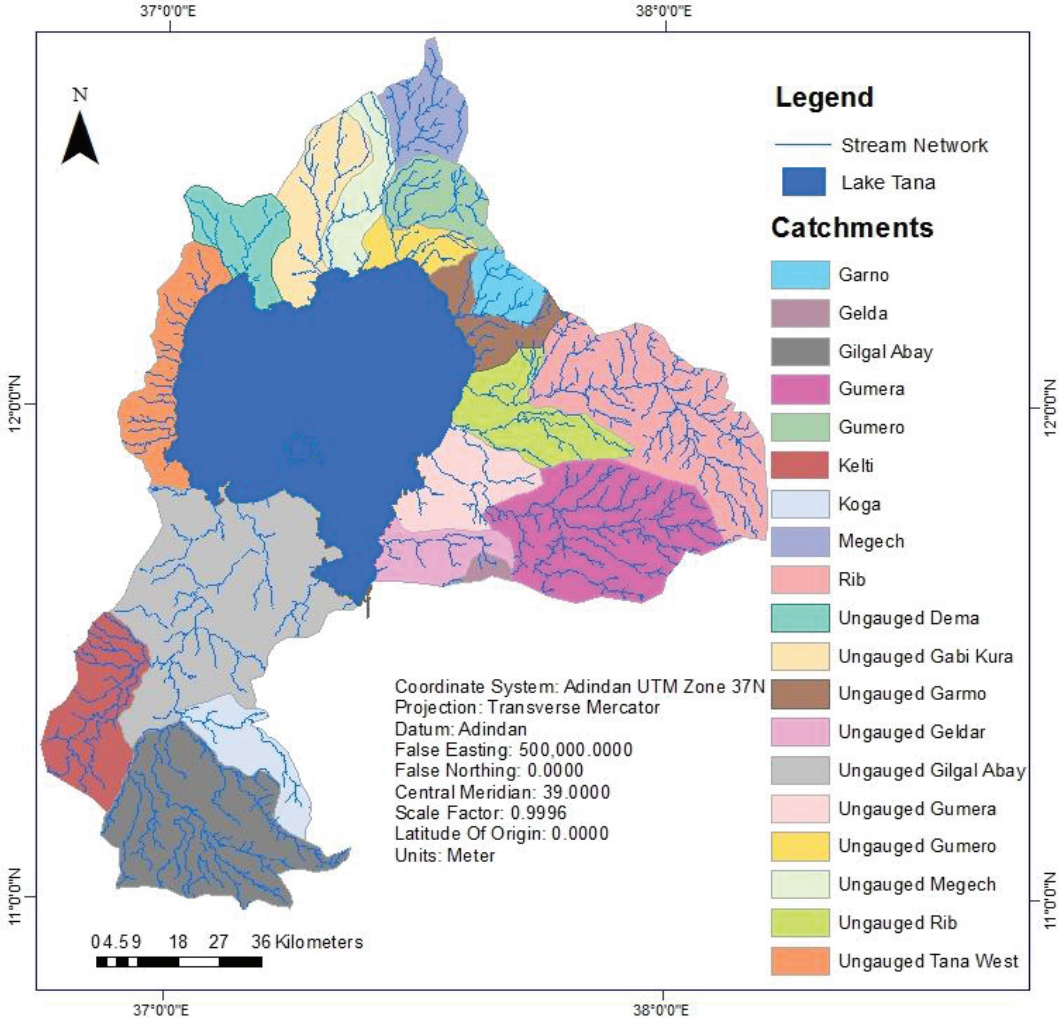

Figure 6: Gauged and ungauged catchments of Lake Tana basin with respective stream network

Lake Tana has more than forty tributary rivers. Major gauged catchments which contributes inflow to the lake are Megech from the northern part of the lake; Gilgel Abbay, Koga and Kelti from the southern part of the lake and Gumera, Gelda, Garno and Ribb from the eastern side of the lake. Their inflows are measured based on actual river discharge while the inflows from ungauged rivers are simulated by HBV model. The summation of all inflow of gauged and ungauged catchments gives total inflow to the Lake Tana. The HBV model structure with its input data required to simulate the discharge is presented in section 2.6.2.

4. METHODOLOGY

4.1. Data Quality Control

4.1.1. Estimation of Missing Rainfall Data

In this study missing rainfall data was estimated by using the rainfall data at neighbouring stations. Missing daily precipitation P_x was estimated based on the procedure proposed in (Subramanya,2008). The missed values of rainfall data estimated by arithmetic mean (see equation 4.1) in a case the normal annual rainfall at any of the neighbouring stations is within 10% of the normal annual precipitation at target station. The normal rainfall is an average value of rainfall over a specified period (e.g. year, month or date). Target station is station with missing data and neighbouring stations are source stations used to estimate missing data. In case the normal annual rainfall at any of the neighbouring stations varies considerably (i.e. more than 10%) from the normal annual precipitation at target station, then the normal ratio method (equation 4.2) is used to calculate the missing value (P_x).

$$P_x = \frac{P_1 + P_2 + P_3 + \ldots + P_n}{n} \quad 4.1$$

$$P_x = \frac{N_x}{n}\left[\frac{P_1}{N_1} + \frac{P_2}{N_2} + \frac{P_3}{N_3} + \cdots + \frac{P_n}{N_n}\right] \quad 4.2$$

Where n is number of neighbouring stations; N_x is normal annual precipitation of the target station; P_1, P_2, $P_3 \ldots P_n$ are daily precipitations of respective neighbouring stations and N_1, N_2,..N_n are annual total precipitations of respective neighbouring stations.

4.1.2. Test for Consistency of data

Consistency of time series data analysed based on theory that a plot of two cumulative quantities that are measured for the same time period should be straight line and their proportionality remain unchanged, which is represented by the slope.

The following procedure is adopted from Hydrological engineering book of (Subramanya,2008). Select the target station X where inconsistency in rainfall records is observed and nearly 5 to 10 neighbouring stations. Arrange both target and neighbouring stations average rainfall time series data in reverse (latest to oldest) chronological order. Then compute target station accumulated precipitation ($\sum P_x$) and neighbouring stations accumulated average precipitation ($\sum P_{av}$) of the latest record. Breaking of the slope of the plot of consecutive period ($\sum P_x$) versus ($\sum P_{av}$) shows a change (i.e. inconsistency) in the precipitation of target station. The change in slope considered as significant only if it persists for more than 5 years. Finally precipitation values beyond the period of breaking of the slope is corrected by using equation (4.3)

$$P_{cx} = P_x \frac{M_c}{M_a} \quad (4.3)$$

Where as P_{cx} is the corrected-precipitation at period at station X; P_x is the original record rainfall for this period at X; M_c is corrected slope of the double mass curve and M_a is the original slope of the mass curve (see Figure 7). In general, when the neighbouring station records are more homogeneous the more accurate will be the corrected values at the target station.

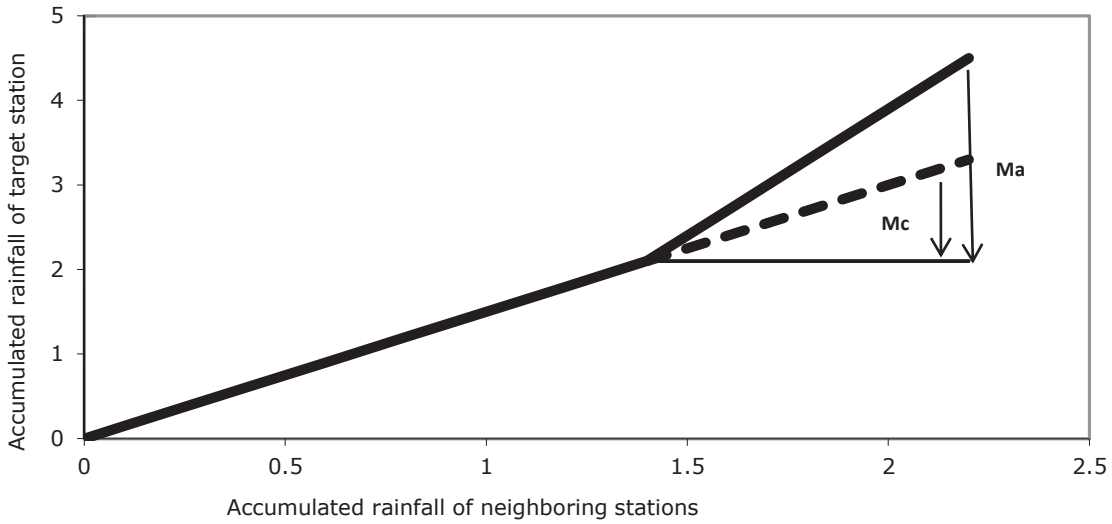

Figure 7: Double mass curve for correction of precipitation inconsistency

4.2. DownScaling climate data

Downscaling climate data was done by using Statistical DownScaling Model (SDSM 4.2). The output of regional climate Model (i.e. CCLM A1B scenario) was collected from IWMI (see section 4.4). The HadCM3 was employed for A2 and B2 emission scenarios. A2 is medium-low emission scenario, B2 is Medium-High emission scenario(IPCC,2012) and A1B scenario is balanced emission scenario.

4.3. Statistical DownScaling

Stastical DownScaling Model (SDSM 4.2) developed by Wilby et al. (2008) was downloaded freely from http://www.sdsm.org.uk. It establishes statistical relationships between output from GCM at large-scale (i.e. predictors) and observed data from meteorological stations at local-scale (i.e. predictands) climate based on multiple linear regression techniques. The predictor variables of HadCM3 Predictors A2 (a) and B2 (a) Experiments which is supplied on a grid box basis is freely downloaded from "Environment Canada" website http://www.cics.uvic.ca/scenarios/sdsm/select.cgi. Letter "a" after both A2 and B2 scenarios refer to a different initial point of climate solution for ensemble members along the reference period. The bordering grid box that represents the Lake Tana is shown in Figure 8 to download the HadCM3 data from African window. The general procedure used to downscale from GCM output data is presented in the flowchart in Figure 9.

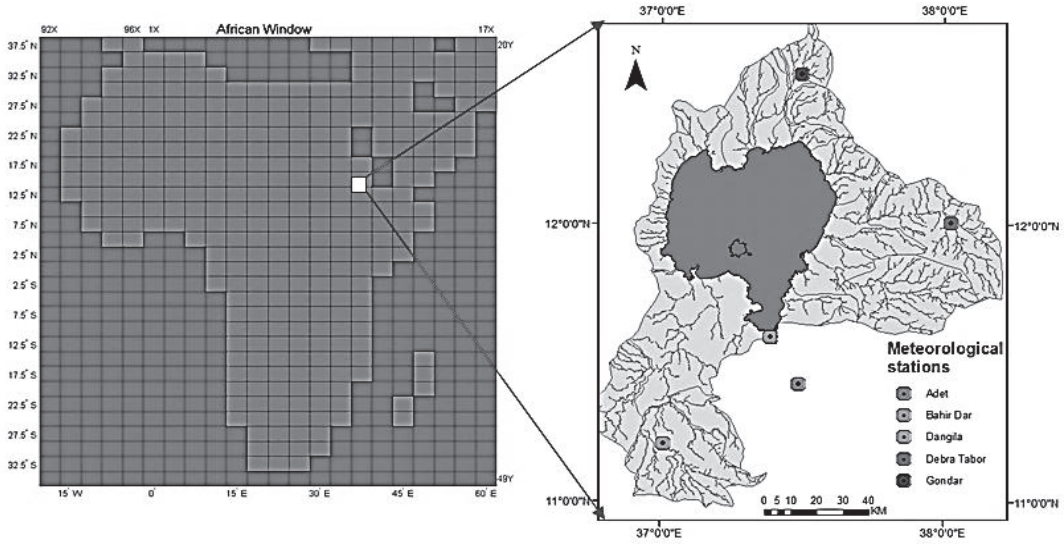

Figure 8: HadCM3 predictors downloading site African window (left side http://www.cics.uvic.ca/scenarios/sdsm/select.cgi) for Lake Tana (right side)

Daily maximum temperature, minimum temperature and precipitation is downscaled by using the following seven discrete processes. These are predictand data quality control; predictor variables selection; model calibration; weather generation; statistical analyses; model output graphic presentation and scenario generation using climate model predictors. The procedures applied in the section below (i.e. 4.2.1 to 4.2.7) were adapted from the SDSM 4.2 manual (Wilby et al.,2008).

4.3.1. Predictand data quality control

Data collected from meteorological stations may not be 100% complete and/or accurate. In SDSM, quality control of time series data is very crucial step to handle missing or imperfect data. For all meteorological stations daily data quality was checked to manage missed, suspected values and outliers of the predictand before screening of the predictor variables.

4.3.2. Screening downscaling predictors

Screening predictors is central and the most challenging stage in statistical downscaling because it determines the character of the downscaled climate Scenario. Its main purpose is to assist the user in the selection of appropriate downscaling predictor variables. In Wilby et al. (2002) selection of predictors in SDSM is described as is an iterative process and partly based subjective judgment of the user's.

In this study, predictors with relatively high partial correlation value and P value less than 0.05 were selected (see Table 9). According Afifi et al. (1996) partial correlation is defined as " the correlation between two variables after removing the linear effect of the third or more other variables". It is calculated by using equation 4.4.

The partial correlation between variable i and j while controlling for third variable k where R_{ij} is correlation coefficient between j and i:

$$R_{ij,k} = \frac{R_{ij} - R_{ik}R_{jk}}{\sqrt{(1-R_{ik}^2)(1-R_{jk}^2)}} \quad (4.4)$$

According Hessami et al. (2008) the p-value is estimated by transforming the correlation 'R' to establish a t-statistic with n-2 degrees of freedom (see equation 4.5 below) and is used to eliminate any one of the predictors in partial correlation method with the n number of observations.

$$t = \frac{R}{\sqrt{\frac{1-R^2}{n-2}}} \quad (4.5)$$

The statistical test (i.e. t-test) used to calculate a p-value, which is used to accept or reject the hypotheses that the two sets of data (i.e. observed and simulated) could have similar or the same Stastical properties. Significant differences between the simulated and observed climate data may be arise from the errors in the observed data, model smoothing of the observed data or random error.

The higher partial correlation values show strong association between predictor and predictand whereas smaller P values indicate that the occurrence of this association is less likely by chance. The partial correlation statistics and P values shows the strength of the association between predictor and predictand. The association strength of individual predictors varies on a monthly basis and the most appropriate combination of predictors was by looking at the analysis output of the twelve months. P value less than 0.05 is consistently used as the cut-off. However, even if P is less than 0.05 the result can be statistically significant but not be of practical significance. When there is high correlation and low P value, the scatter plot was used to evaluate whether this result is due to few outliers, or is a potentially useful downscaling relationship. The Scatter plot may also reveal that one (or both) of the variables should by modified using the "transform operation", to make linear relationship.

Table 5: Large-scale atmospheric variables (Predictors) which are used as potential inputs in SDSM

No.	Predictors	description	No.	predictors	description
1	tempaf	mean temperature at 2 m	14	p500af	500hpa geo-potential height
2	shumaf	surface specific humidity	15	p5_zaf	500hpa vorticity
3	rhumaf	near surface relative humidity	16	p5_vaf	500hp meriodinal velocity
4	r850af	relative humidity at 850hpa	17	P5_ zhaf	500hpa divergence
5	r500af	relative humidity at 500 hpa	18	p5_uaf	500pa zonal velocity
6	p8zhaf	850 hpa divergence	19	p5_faf	500hpa air flow strength
7	p8thaf	850hpa wind direction	20	p_zhaf	surface divergence
8	p850af	850hpa geo-potential height	21	p_zaf	surface vorticity
9	p8_zaf	850 hpa vorticity	22	p_vaf	surface meridian velocity
10	p8_vaf	850 hpa meriodinal velocity	23	p_uaf	surface zonal velocity
11	p8_uaf	850hpa zonal velocity	24	p_thaf	surface wind direction
12	p8_faf	850hpa airflow strength	25	p_faf	surface air flow strength
13	p5thaf	500hpa wind direction	26	mslpaf	men sea level pressure

The predictor variables are normalized with respect to their 30 years (1960-1990) means and standard deviations. (Source: http://www.cics.uvic.ca/scenarios/index.cgi?More_Info-SDSM_Background , accessed on November 13, 2012)

4.3.3. SDSM Model Calibration

By calibrating of the SDSM, the downscaling model is build based on multiple linear regression equations, daily predictand data (i.e. meteorological station data) for GCM predictor variables. In this study calibration is done by using selected Screen Variables (see Table 5) and level of the variance in the local predictand of daily precipitation, maximum and minimum temperature of Gondar, Bahir Dar, Debra Tabor, Aykel, Dangila and Adet stations data for the period of 1961-1990 are used. This 30 period is served as the baseline for this study.

During model calibration, stepwise regression for precipitation while unconditional process for maximum and minimum temperature was applied. In stepwise regression initially all predictors are included during predictor screening and during the analysis least significant terms are removed at every step. In

unconditional process, a direct link assumed between the predictors and predictand whereas conditional processes are done with intermediate process. For each station, the model calibration result is checked by visual inspection (i.e. frequency analysis output graphs of the model output versus the observed) and statistical methods (i.e. statistical summary of model output versus observed) to now the skill of the model to reproduce the genuine scenario data.
According to (Wilby et al.,2002) the calibration result of SDSM is exhibited with percentages of explained variance. The equation used to define percentage of the explained variance (%ev) provided by (Vrac et al.,2012) as follows (see equation 4.6).

$$\%ev = \frac{\sum_{i=1}^{n}(S_i - \bar{O})}{\sum_{i=1}^{n}(O_i - \bar{O})} \times 100 \quad (4.6)$$

Where S_i is the simulated value for day i, O_i is the observed value at day i, $\bar{O}$ is the mean of the observations for the period and n is the number of days of the period of SDSM run and observed data. The percentage of explained variance used to describe the variability of the simulated data with respect to the mean of the observations. In another word, it is report of calibration result that provided by SDSM algorithm to show the extent to which the regional predictors determine the daily variations of local predictand.

The SDSM calibration result of previous studies (see Table 6) indicates the percentage of explained variance is higher for temperature (i.e. s spatially less variable) than precipitation. It is not possible to limit an 'acceptable' level of explained variance, because SDSM model skill differs for different geographical locations, even for a common set of predictors.

Table 6: Summary of calibration result of SDSM from previous studies

Precipitation	Minimum temperature	Maximum temperature	Study area	Authors
28%	72%	73%	Toronto	(Wilby et al.,2002)
15% to 45%	70% to 90%	70% to 90%	Mountainous regions of Japan	(Wilby et al.,1998)
6% to 10%	71% to 79%	71% to 79%	Greater Montréal region	(Nguyen et al.,2004)
38%	55%	62%	Upper Blue Nile Basin Ethiopia	(Bekele,2009)

4.3.4. Scenario Generation

The Scenario Generation process produces daily base data for maximum temperature, minimum temperature and precipitation for the period 1960-2099 and for the future time windows. Each predictand (i.e. precipitation, maximum and minimum temperature) scenario is generated based on the calibration result and the daily atmospheric predictors of the HadCM3 (see Table 5). The calibration result is used based on assumption that predictor-predictand relationships under the current condition remain valid under future climate conditions too.

HadCM3 has two emission scenarios B2 and A2. For each emission, scenario twenty ensembles of synthetic daily time series data were produced for 139 years. As explained in detail at "Canada Environment" website http://www.cics.uvic.ca/scenarios/index.cgi, the stochastic component of SDSM allows the generation of up to 100 ensembles. Where ensemble data has the same statistical characteristics but vary on a day-to-day basis. Selection of only twenty ensembles is done due to reasonably match between observed and simulated daily temperature and precipitation. In addition, large number of ensembles notably did not improve and subjective for large deviation among ensembles output, only 20 individual ensemble outputs are averaged to improve the performance of model for future time horizon.

For three future time horizons 2010-2039(2020s), 2040-2069(2050s) and 2070-2099(2080s) the A2 and B2 emission scenarios precipitation, maximum and minimum temperature outputs are generated.

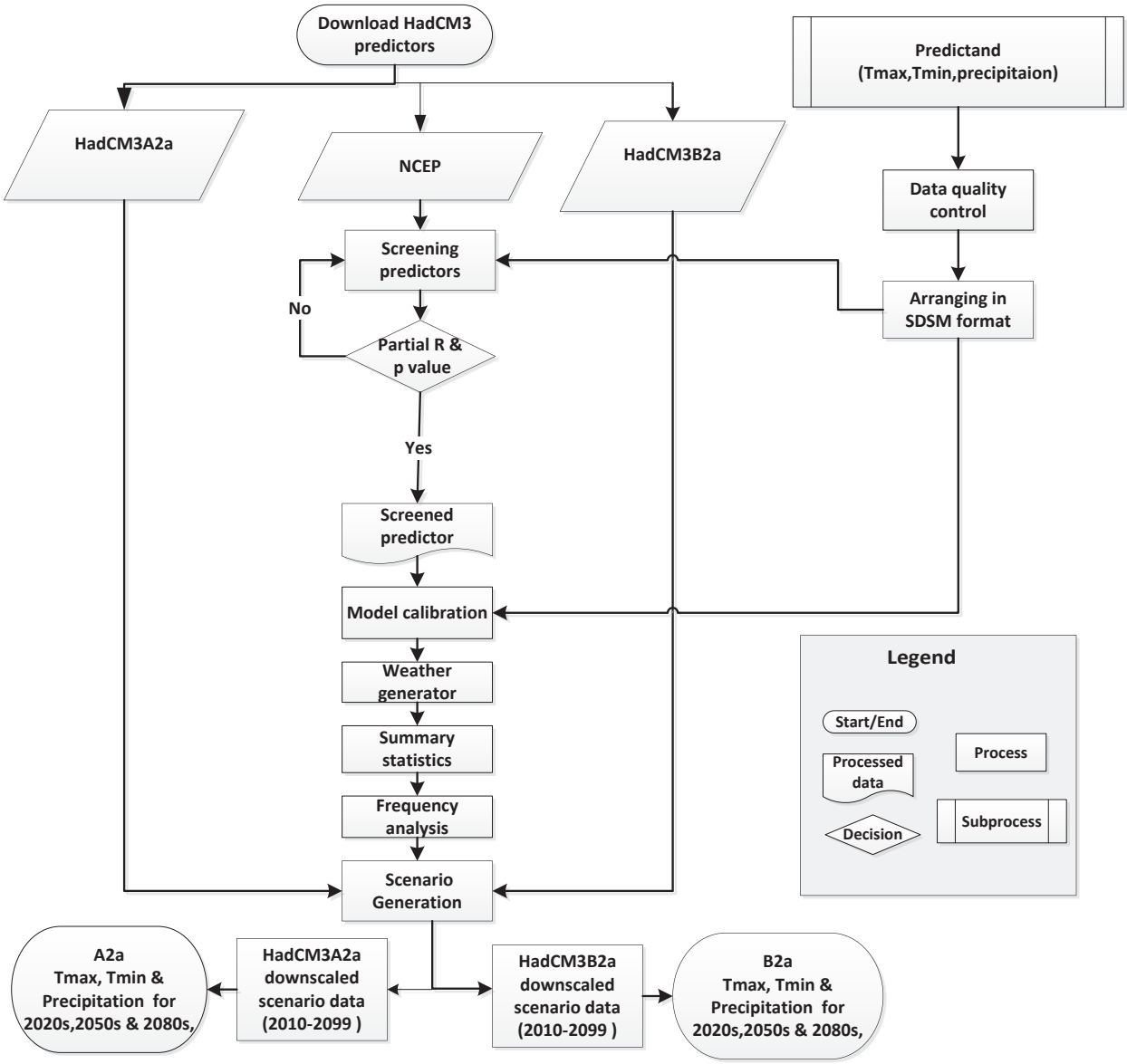

Figure 9 : DownScaling methodology of Statistical Downscaling Model (SDSM 4.2)

4.4. Regional Climate Model

In this study, outputs from the regional climate model CCLM were used. CCLM is abbreviation for "COSMO-Climate Limited-area Modelling" and COSMO stands for COnsortium for "Small scale Modelling". CCLM as a non-hydrostatic regional climate model (RCM) that is developed by the German Weather Service (Nguyen et al.,2004). The non-hydrostatic component offers the opportunity to represent convictive movements. CCLM model covers the whole of Europe and the African regions bordering the Mediterranean Sea with horizontal model resolution between 1 and 50km and temporal resolution between 1 day to 1 hour (Gagnon et al.,2005).

Currently, the Potsdam Institute for Climate Impact Studies (PIK) operates CCLM. Downscaling with forcing GCM of the ECHAM5 for A1B emission scenario and the first round bias correction is done by global reanalysis data by PIK. These first round bias corrected data is collected from International Water resource research institute (IWMI) Ethiopia. Further bias correction for precipitation and temperature for stations over the study was needed.

Despite of high-resolution climate data provision, the RCM technique has its own limitations. The main limitations of the RCM technique are systematic errors (Berg et al.,2012) in the driving fields provided by global models; the lack of two-way interactions between regional and global climate; computationally demanding; and need of careful co-ordination between global and regional modellers to perform RCM experiments. These theoretical and practical limitations may cause bias and should be corrected either by delta approach, linear-scaling approach or mean correction method (Teutschbein et al.,2012). Delta change approach is commonly used RCM output bias correction method that developed by (Hay et al.,2000) and has been used in many climate change impact studies (Akhtar et al.,2008; Kling et al.,2012; Yang et al.,2010) but it works at monthly basis. Consequently, for this study Linear-scaling approach is selected because it works at daily basis that agrees with daily simulation of HBV model.

The Linear-scaling approach(Teutschbein et al.,2012) is adopted for this study due to its suitability for bias correction at daily basis. From observed climate time series RCM simulation is adapted with estimated daily mean for each future time horizons. Observational data from 1980 to 2010 is calculated at daily mean basis. The future daily bias corrected temperature ($T^*_{RCM,daily}$) and daily precipitation ($P^*_{RCM,daily}$) time series will be built by using equations 4.7 and 4.8 respectively.

$$T^*_{RCM,daily} = T_{RCM,daily} + (\overline{T_{obs,daily}} - \overline{T_{RCM,daily)}}) \quad (4.7)$$

$$P^*_{RCM,daily} = P_{RCM,daily}\left(\frac{\overline{P_{obs,daily}}}{\overline{P_{RCM,daily}}}\right) \quad (4.8)$$

Where: $\underline{T_{RCM,daily}}$ is daily RCM simulated temperature data,
$\overline{T_{RCM,daily}}$ is mean daily RCM simulated temperature for respective time horizons,
$\overline{T_{obs,daily}}$ is mean daily observed temperature for the period of 1981 to 2010,
$\underline{P_{RCM,daily}}$ is daily RCM simulated precipitation,
$\overline{P_{obs,daily}}$ is the mean daily observed precipitation for the period of 1981 to 2010 and
$\overline{P_{RCM,daily}}$ is the mean daily RCM simulated precipitation for respective time horizons (i.e. 2020s, 2050s and 2080s).

According to Teutschbein et al. (2012) mean monthly values of the observed ground truth data and corrected RCM simulations perfectly agree with long term mean. However, this perfect agreement depends on the area of study and for Lake Tana it is not yet checked. Precipitation is corrected with a factor based on the ratio of long-term mean monthly observed and control simulation and temperature is corrected with an additive term based on the difference of long-term mean monthly observed and RCM simulation data. The correction factors used and addends applied are assumed to remain the same even for future conditions.

4.5. Lake Evaporation and precipitaion

4.5.1. Overlake Precipitation

Over-Lake daily precipitation for the period 1980-2010 was estimated through inverse distance weighted interpolation method. Five stations located inside or close to the lake are selected (see Figure 10). The

equation used for inverse distance weight is explained in equation (4.9) below. As indicated in Haile et al. (2009) weight power of 2 represents better spatial variability when compared to smaller values.

$$P_x = \frac{\sum_{i=1}^{N} \frac{1}{(d_i^2)} P_i}{\sum_{i=1}^{N} \frac{1}{(d_i^2)}} \quad (4.9)$$

Where: P_x= estimate of over-lake rainfall
P_i= rainfall values of individual rainguage stations used for estimation
d_i= distance between each location to the point being estimated
N = Number of surrounding stations
2= distance weight
d_i = distances from each location to the interpolation point and given by:

$$di = \sqrt{(x - x_i) + (y - y_i)}$$

Where (x, y) are the coordinates of the interpolation point of the lake and (x_i ,y_i) are the coordinates of each station location (see Figure 10) around the lake. When the distance from location of each station increases away from interpolation point, the weight function closes to zero. The station weight functions are normalized and their sum is equal to one.

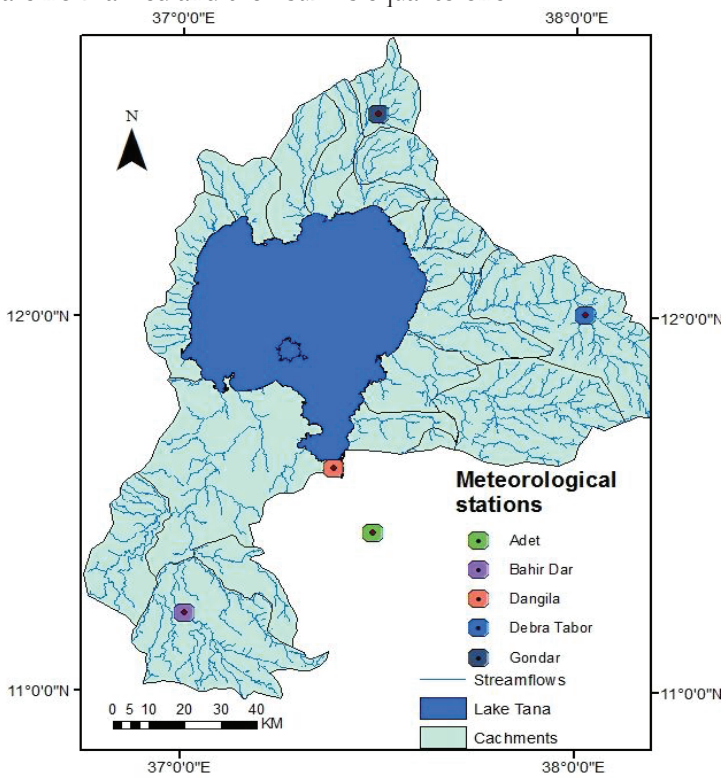

Figure 10 : Stations for estimation of evaporation, evapotranspiration and precipitation

4.5.2. Lake evaporation

Lake evaporation for period of 1981-2010 was calculated by using the Penman-combination method (see equation 5). The estimated lake evaporation used to describe the study area but it is not used for emission scenario analysis. Climatological record data is collected from National Meteorological Agency (NMA) of Ethiopia for the period of 1981-2010. The standard climatological records of daily sunshine hours, temperature, humidity and wind speed are inputs to compute the evaporation from open water surface. In Maidment (2010) energy balance combined with a water vapour transfer of Penman-combination equation is used to calculate open water evaporation for the baseline period to describe the study area.

$$E_p = \frac{\Delta}{\Delta+\gamma} * (R_n + A_h) + \frac{\gamma}{\gamma+\Delta} * \frac{6.43*(1+0.536u_2)*D}{\lambda} \quad (5)$$

Where E_p = potential evaporation from the lake surface (mm/day), R_n = the net radiation exchange for the free water surface (mm/day), A_h = the energy advected to the water body (mm/day), u_2 = the wind speed measured at 2 meter a.s.l (m/s), D = the average vapour pressure deficit (kPa), λ = the latent heat of vaporization (MJ/kg) and γ = Psychrometric constant (KPa^{0}C).

$$R_a = \frac{24(60)}{\pi} G_{sc}\, d_r[\omega_s \sin(\varphi) + \cos(\varphi)\cos(\delta)\sin(\omega_s)] \quad (5a)$$

Where R_a=Extraterrestrial radiation [MJ m^{-2} day^{-1}], G_{sc} =Solar constant = 0.0820 MJ m^{-2} min^{-1}, d_r = Inverse relative distance Earth-Sun, ω_s =Sunset hour angle [rad], Φ =Latitude [rad] and δ = Solar declination [rad].

The corresponding equivalent evaporation in mm day^{-1} is estimated by multiplying R_a and 0.408 (Equation5a). The latitude, φ, expressed in radians is negative for the southern hemisphere and positive for the northern hemisphere. The conversion from decimal degrees to radians is given by:

$$[\text{Radians}] = \frac{\pi}{180}\,[\text{decimal degrees}] \quad (5b)$$

In the FAO Penman-Monteith equation (Equation 5), radiation expressed in MJm^{-2}day^{-1} is converted to equivalent evaporation in mmday^{-1} by using a conversion factor equal to the inverse of the latent heat of vaporization (1/λ= 0.408):

$$\text{Equivalent evaporation [mm/day]} = 0.408*(\text{Radiation})\ [\text{MJm}^{-2}\text{day}^{-1}] \quad (5c)$$

The inverse relative distance Earth-Sun,d_r, and the solar declination, δ , are given by:

$$d_r = 1 + 0.033\cos(\frac{2\pi}{365} J) \quad (5d)$$

$$\delta = 0.409\sin(\frac{2\pi}{365}J - 1.39) \quad 5e)$$

J is the number of the days in the year between 1 (1st January) and 365 or 366 (31st December) at leap year. The sunset hour angle (ω_s) is given by:

$$\omega_s = \arccos[-\tan\varphi\ \tan\delta] \quad (5f)$$

The psychometric constant γ is given on equation (5g) which is dependent on atmospheric pressure P [kPa]. Atmospheric pressure is also function of elevation above sea level [m].

$$\gamma = \frac{C_p P}{\varepsilon\lambda} = 0.665\text{x}10^{-3}P \quad (5g)$$

Where: γ Psychrometric constant [kPa °C-1]; $P = 101.3\left(\frac{293-0.0065z}{293}\right)^{5.26}$ is atmospheric pressure [kPa]; λ=2.45 [MJ kg-1] is latent heat of vaporization; C_p=1.013x10-3[MJ kg^{-1}°C^{-1}] is specific heat at constant pressure and ε = 0.622 is the ratio molecular weight of water vapour/dry air.

The relative humidity (RH) shows the degree of saturation of the air and it is ratio of the actual (e_a) to the saturation ($e^o(T)$) vapour pressure at the same temperature and (see equation 5h)

$$RH = \frac{e_a}{e^o(T)} \quad (5h)$$

Relative humidity is used to calculate saturation vapour pressure that depends on air temperature and, it can be calculated from the air temperature. The relationship is presented in equation 5i and 5k below.

$$e^0(T) = 0.6108\exp\left[\frac{17.27T}{T+2737.3}\right] \quad (5i)$$

$$e_s = \frac{e^o(Tmax)+e^o(Tmin)}{2} \quad (5k)$$

Where e° (T) is saturation vapour pressure at the air temperature T [kPa] and T is air temperature. For the calculation of evapotranspiration, the slope of the relationship between temperature and saturation vapour pressure Δ is required

$$\Delta = \frac{4098\left[0.108\exp\left(\frac{17.27T}{T+237.3}\right)\right]}{(T+237.2)^2} \quad (5l)$$

Where Δ is slope of saturation vapour pressure curve at air temperature T [kPa°C^{-1}] and T is air temperature [°C].

The daylight hours (N) is given by: $N = \frac{24}{\pi}\omega_s$ (5m)

Where ω_s is the sunset hour angle in radians given by Equation (5) and mean values for N (15th day of each month) for different latitude.

Albedo estimated from MODIS level 1(http://ladsweb.nascom.nasa.gov/data/search.html) product and calculated from channels 1 to 7 by integrating band reflectance across the shortwave spectrum. Images require geometric, radiometric and atmospheric correction and the radiance at the top of the atmosphere needs to be known. During integration, weighting coefficients are applied that represent the fraction of surface solar radiation occurring within the spectral range as represented by a specific band. Detailed procedures are explained in (Kibret,2009).

4.5.3. Catchment evapotranspiration

Catchments evapotranspiration from for baseline period 1981-2010 and future time horizons (2011-2099) is calculated by Hardgrave's method Hargreaves et al. (1982) (see equation 2.4). The Hardgrave's equation is a temperature based method and although it has a link to solar radiation.

$$E_{rc} = 0.0022 * R_a * \delta'T^{0.5} * (T + 17.8) \quad (5.1)$$

Where: R_a is mean extra-terrestrial radiation [mm/day], which is a function of the latitude f, $\delta'T$ is temperature difference (i.e. mean monthly maximum temperature minus mean monthly minimum temperature for the month of interest [^{0}C] and T is mean air temperature [^{0}C]. This equation gives reasonable estimates of reference crop evapotranspiration because it has a link to solar radiation through Ra and takes into account the impact of radiation warming the surface near the ground.

For current and future time horizon, (1981-2099) lake evaporation was estimated by using Hargreaves method (see equation 5.1) due to non–availability of daily sunshine hours, humidity, wind speed and albedo for future periods. The only available data were maximum and minimum temperature that downscaled by SDSM and bias corrected RCM outputs.

4.6. Hydrological impacts of climate change and hydrological modeling

Downscaled SDSM and RCM climate scenarios consist of maximum and minimum temperature and precipitation together with an estimated potential evaporation used as input to the HBV model. According to (Burger et al.,2007) bias in RCM simulated variables can lead to unrealistic hydrological simulations and thus RCM outputs need modification for bias correction . In this study, RCM output bias corrected and downscaled SDSM outputs are used as input for hydrological models to represent the future climate.

For hydrological modelling of climate change impacts, the HBV-96 is used to simulate stream flow for future climate scenario. The model consists of subroutines for atmospheric condition, soil moisture accounting procedures and runoff generation routines (see Figure 11). Its flexible structure to create sub-divisions with respect to sub-basins and climatic zone makes it suitable for this study. It is possible to run, calibrate and validate the model separately for several sub-basins (SMHI,2006) and to simulate runoff

from the entire sub-basins. Input data such as daily precipitation, temperature and potential evaporation have been kept as simple as possible.

Where:

SF: Snowfall,
RF: Rainfall,
EI: Evapo-transpiration,
IN: Infiltration,
EA: Actual Evaporation,
FC: Maximum soil moisture storage,
SM: compound soil moisture routine,
CF: capillary rise,
R: seepage,
UZ: upper zone reservoir,
Qo: direct runoff from upper reservoir,
EL: lake evaporation,
PERC: percolation capacity,
LZ: lower zone reservoir and
Q1: base flow lower reservoir.

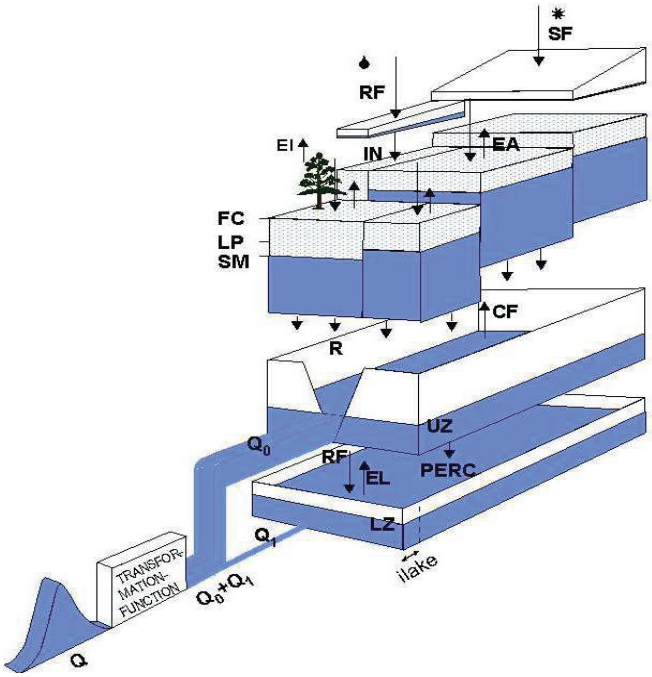

Figure 11: Schematic presentation of the HBV model for one sub-basin (SMHI,2006)

The overall water balance of HBV-model is described in equation (5.2) below.

$$\frac{d}{dt}(SP + SM + UZ + LZ + Lake) = P - Q - E \quad (5.2)$$

Where P is Precipitation, Q is Runoff,
SP is Snow pack, SM is Soil moisture,
UZ is Upper groundwater Zone and
LZ is Lower groundwater Zone and Lake is reservoir volume

Calibration and validation of the model for the period 1994-2000 for all gauged and ungauged catchments is done by (Perera,2009). HBV model code developed by ITC WREM department based on the HBV-96 version with the Computer language MATLAB. Formerly HBV model is written in FORTRAN for the Meuse basin by Booij (2005) and adjustments were made to the model based on the preferred catchment, model parameters, routing routine and model calibration method.

The total inflow to the lake is estimated from gauged and ungauged catchments by summing the inflows from all catchments. The inflow from each catchment is simulated based on downscalled SDSM and RCM bias corrected data (i.e daily precipitation, mean temperature and evaporation) of stations arround the Lake Tana. Inverse distance weighting method is used to calculate weight of each station (see Table 7 and Table 8) to the catchment, which is presented in Figure 5. The unit of precipitation and the evaporation is mm/day, inflow from catchment which is simulated in m^3/s multiplied by the factor 86.4 and divided by catchment area to convert m^3/s to mm/day to make units of water balance component the same.

Table 7: Weight of precipitation and evaporation stations for the gauged catchments

Gauged catchments	Meteorological stations				
	Adet	Bahir Dar	Debra Tabor	Dangila	Gondar
Gelda		0.65	0.35		
Koga	0.45	0.28		0.27	
Gumero			0.25		0.75
Garno			0.40		0.60
Kelti				1.00	
Megech					1.00
Gilgal Abay	0.40			0.60	
Gumera		0.21	0.79		
Ribb			1.00		

Table 8: Weight of over-lake precipitation and evaporation stations for the ungauged catchments

Ungauged catchments	Meteorological stations				
	Adet	Bahir Dar	Debra Tabor	Dangila	Gondar
Ribb		0.4	0.6		
Gilgal Abay	0.27	0.43		0.3	
Garno			0.47		0.53
Gelda		0.78	0.22		
Gumera		0.63	0.37		
Gumero					1.00
Megech					1.00
Dema					1.00
Tana West		0.49			0.51
Gabi Kura					1.00

The analysis of water balance is carried out in three time horizons in future period each covering non-overlapping 30 years period. These periods consist of 2020s (2011-2040), 2050s (2041-2070) and 2080s (2071-2100). The overall water balance equation that used to investigate the hydrological impact of climate change is described in equation (5.3) that estimates water balance at daily basis.

$$\frac{\Delta S}{\Delta t} = P + Q_{gauged} + Q_{ungauged} - E - Q_{out} \quad (5.3)$$

Where: $\Delta S/\Delta t$ is the change in storage over time [Mm^3/day],
P is the lake's areal rainfall of past records and RCM scenario outputs [Mm^3/day],
E is the open water evaporation of past records and RCM scenario outputs [Mm^3/day],
Q_{gauged} is the gauged catchments inflow estimated by HBV based on past records and RCM scenario outputs [Mm^3/day],
$Q_{ungauged}$ is the ungauged catchments inflow estimated by HBV based on past records and RCM scenario outputs [Mm^3/day] and
Q_{out} is the Blue Nile River outflow [Mm^3/ day].

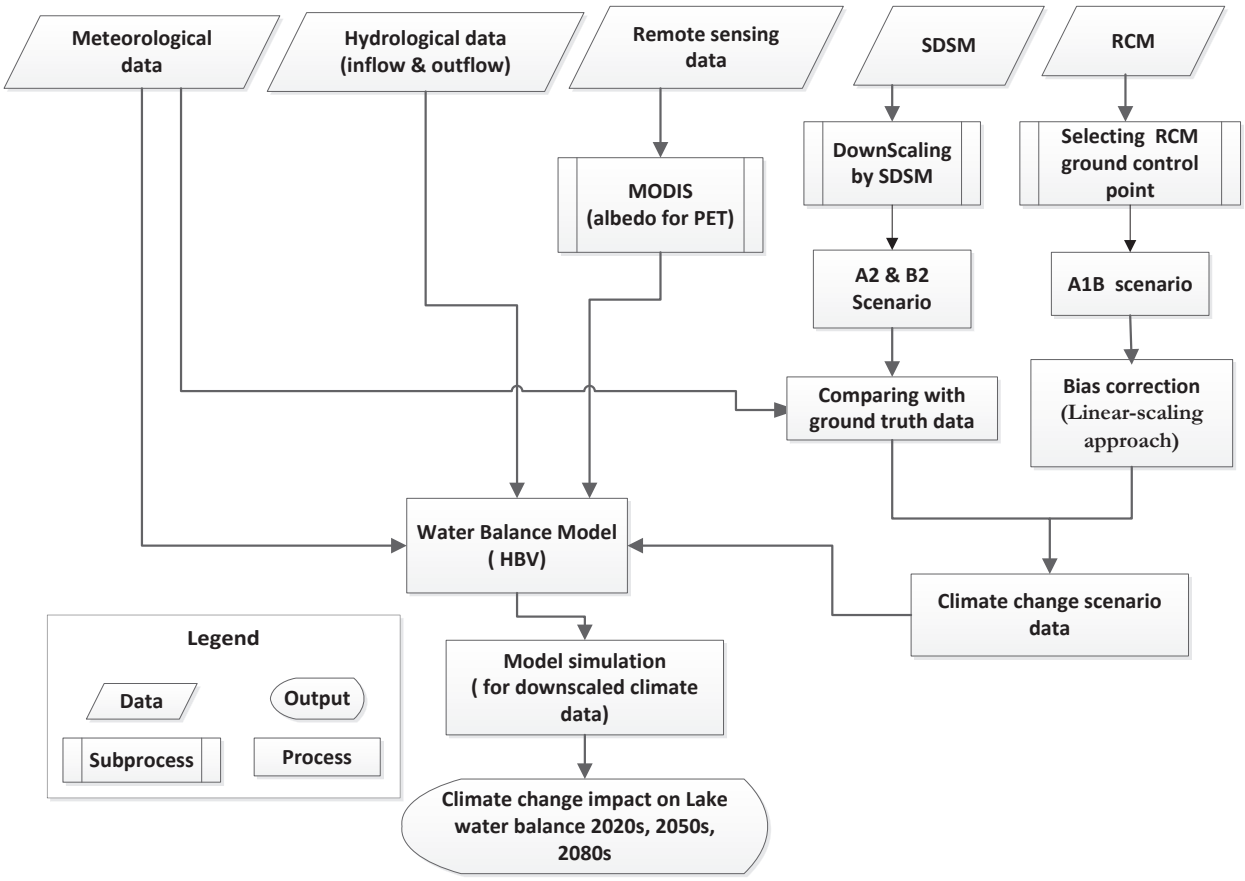

Figure 12: Conceptual framework of research

The overall procedures applied in this study are described in conceptual framework (see Figure 12). Regionalization result from the study of (Perera,2009) is used as input for this study.

5. RESULT AND DISCUSION

5.1. SDSM calibration and RCM bais correction

Predictors of NCEP are presented at Table 9 that are selected to calibrate SDSM model. Screening was done based on partial correlation value and p-value (see explanation in section 4.2.3).

Table 9: Selected predictors for four stations at predictor screening process

Dangila Station				Bahir Dar station			
Predictand	Predictors	Partial r	P-values	Predictand	Predictors	Partial r	P-values
Maximum Temperature	Ncep8_vaf.dat	0.317	0.00	Maximum Temperature	Ncepp500af.dat	0.548	0.00
	Nceptempaf.dat	0.259	0.00		Ncepp8_vaf.dat	0.398	0.00
	Ncepshumaf.dat	0.177	0.00		Nceptempaf.dat	0.346	0.00
	Ncepp500af.dat	0.172	0.00		Ncepshumaf.dat	0.259	0.00
	Ncepp_zaf.dat	0.170	0.00		Ncepp_uaf.dat	0.187	0.00
Minimum Temperature	Ncepp500af.dat	0.324	0.00	Minimum Temperature	Ncepshumaf.dat	0.464	0.00
	Ncep850af.dat	0.216	0.00		Ncepp500af.dat	0.409	0.00
	Nceptempaf.dat	0.192	0.00		Ncepp_uaf.dat	0.271	0.00
	Ncepp_uaf.dat	0.143	0.00		Nceptempaf.dat	0.250	0.00
	Ncepp8_uaf.dat	0.125	0.00		Ncepp8zhaf.dat	0.186	0.00
Precipitation	Ncepp8zhaf.dat	0.268	0.00	Precipitation	Ncep8zhaf.dat	0.218	0.00
	Ncep8_uaf.dat	0.083	0.00		Ncepp8_faf.dat	0.095	0.00
	Ncepp_faf.dat	0.083	0.00		Nceppr500af.dat	0.085	0.00
	Nceppthaf.dat	0.080	0.00		Ncepp8_uaf.dat	0.065	0.00
	Nceppr500af.dat	0.072	0.00		Ncepp5thaf.dat	0.065	0.00
Gondar Station				**Debra Tabor station**			
Predictand	Predictors	Partial r	P-values	Predictand	Predictors	Partial r	P-values
Maximum Temperature	Ncepp8_vaf.dat	0.441	0.00	Maximum Temperature	Ncepp8_vaf.dat	0.281	0.00
	Nceptempaf.dat	0.272	0.00		Nceptempaf.dat	0.249	0.00
	Ncepshumaf.dat	0.262	0.00		Ncepp8_zaf.dat	0.174	0.00
	Ncepp500af.dat	0.250	0.00		Ncepp8_uaf.dat	0.111	0.00
	Ncepp8_zaf.dat	0.208	0.00		Ncepshumaf.dat	0.089	0.00
Minimum Temperature	Nceptempaf.dat	0.321	0.00	Minimum Temperature	Ncepp500af.dat	0.456	0.00
	Ncepp500af.dat	0.300	0.00		Nceptempaf.dat	0.245	0.00
	NcepP8_uaf.dat	0.233	0.00		Ncepp850af.dat	0.223	0.00
	NcepPr500af.dt	0.143	0.00		Ncepshumaf.dat	0.141	0.00
	Ncepp_uaf.dat	0.117	0.00		Ncepp8_uaf.dat	0.140	0.00
Precipitation	Ncepp_vaf.dat	0.035	0.00	Precipitation	Ncepp8zhaf.dat	0.227	0.00
	Ncepp8_uaf.dat	0.047	0.00		Ncepp850af.dat	0.086	0.00
	Ncepp8zhaf.dat	0.084	0.00		Ncepp8_uaf.dat	0.086	0.00
	Nceppr500af.dat	0.042	0.00		Ncepmslpaf.dat	0.068	0.00

The percentage of explained variance is higher for temperature than precipitation because the study of Gagnon et al. (2005) as indicated temperature is spatially more homogeneous than precipitation. The calibration result at Debre Tabor station is 81 % for maximum temperature, 71% for minimum temperature. The percentage of explained variance of precipitation at Debra Tabor (35%), Dangila (29%), Dangila (29%), Bahir Dar (21%), Gondar (19%) and Adet (17%) was found. This calibration result is

reasonably acceptable when it is compared with calibration result of previous studies that presented in Table 6.

In Figure 13 and Figure 14 bias corrected (RCM-corr) and uncorrected RCM (RCM-uncorr) shown for Bahir Dar and Gondar stations. RCM bias correction is done for A1B scenario minimum and maximum temperature, which shows significant difference from bias uncorrected mean monthly when compared with mean monthly-observed data. The deviation of maximum and minimum temperature between corrected and uncorrected RCM is 0.3°C to 1.6°C and 2°C to 4°C at Bahir Dar station; meanwhile at Gondar station it is 0.1°C to 1.1°C and 1.8°C to 4.8°C respectively. This result indicates that using the RCM output without doing bias correction may lead to enormous uncertainty of hydrological analysis.

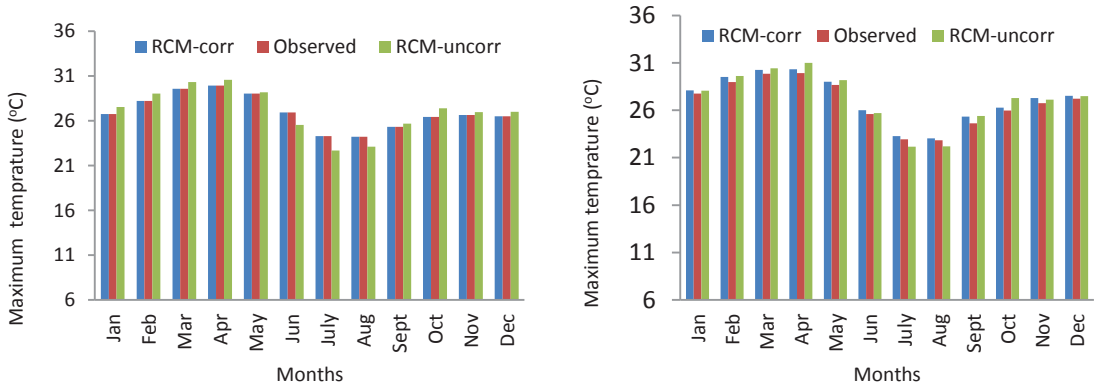

Figure 13: Comparison of RCM bias corrected and RCM uncorrected mean monthly maximum temperature with observed at Bair Dar (left side) and Gondar (right side) stations

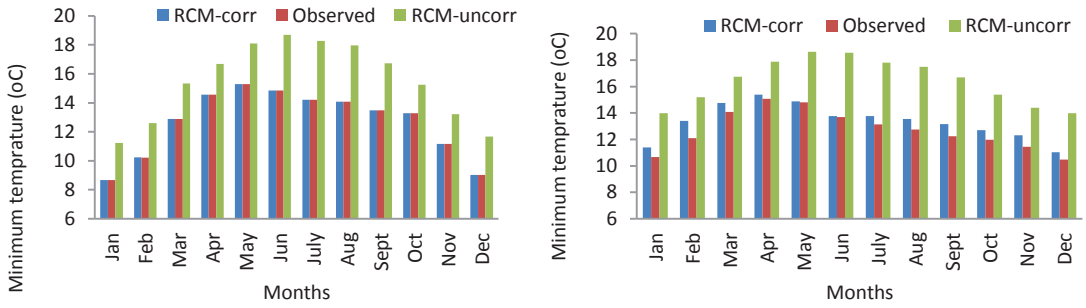

Figure 14: Comparison of RCM bias corrected and RCM uncorrected mean monthly minimum temperature with observed at Bahir Dar (left side) and Gondar (right side) stations.

5.2. Evaluating the performance of SDSM and RCM simulations against observed

Downscaling is conducted for precipitation, maximum and minimum temperature based on data of Bahir Dar, Gondar, Adet, Dangila and Debra Tabor stations for the period of 1961-2099. Based on availability of meteorological station data and consecutiveness for future windows, the baseline period used for this study is 1981-2010. The SDSM (i.e. A2 and B2 scenario) and RCM (i.e. A1B scenario) model output performance is evaluated based on comparison of historic (observed) baseline period 1981-2010. Daily mean downscaled SDSM, RCM output and observed precipitation, maximum and minimum temperature is compared to check whether the historic (observed) condition can be replicated or not (see section 5.1.1-

5.1.3). Therefore, it is vital that model simulated precipitation and temperature data should have the same statistical properties as observed meteorological time series data.

5.2.1. Comparison of RCM and SDSM simulated against observed maximum temperature

The daily mean maximum temperature estimate ranges from 20°C to 29.6°C at Bahir Dar and 20°C to 30.2°C at Gondar station (see Figure 15). The simulated SDSM and RCM bias corrected output indicated reasonable agreement with observed daily maximum temperature. Gondar station RCM simulation shown insignificant difference at warmer season (February to April) by overestimating approximately 0.4°C and 0.5°C (September to December) against observed. For Bahir Dar station SDSM simulation shown inconsequential underestimation roughly 0.5°C (April to August) and 0.6°C (November to December) against observed.

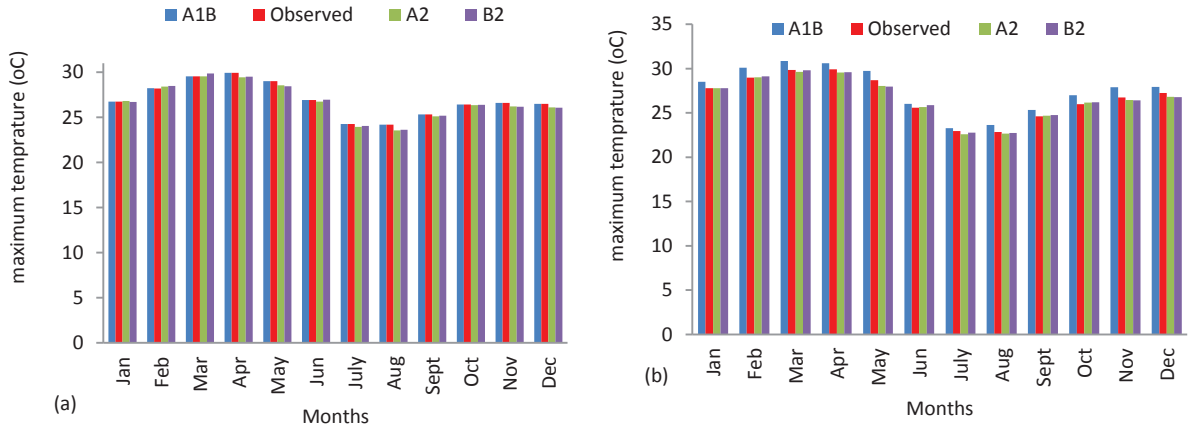

Figure 15: Mean monthly maximum temperature (1981-2010) at Bahir Dar (b) and Gondar (a) stations

The difference between observed and simulated mean monthly maximum temprature is higher at Gondar staion than Bahir Dar staion particularly A1B emission scenario.

The highest maximum temperature based on downscaled and observed data is in the month of March – April and is approximately 29.6 and 29.9°C at Bahir Dar and Gondar stations respectively. The lowest maximum temperature is in the month of July – August approximately 24.2°C at Bahir Dar and 22.8°C at Gondar stations.

5.2.2. Comparison of minimum temperature of RCM and SDSM simulated against observed

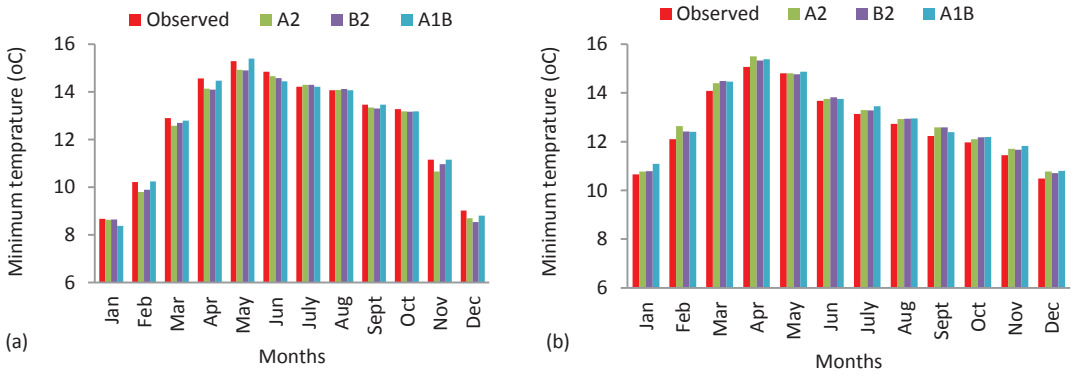

Figure 16: Mean monthly minimum temperature (1981-2010) at Bahir Dar (a) and Gondar (b) stations

The downscaled SDSM and RCM bias corrected mean monthly minimum temperature indicated reasonable agreement with observed mean monthly data. RCM simulations shown insignificant difference from observed by overestimating approximately 0.1 to 0.4°C (February to April) and 0.5°C (September to December) at Gondar station (see Figure 16). Meanwhile it also shows underestimation of 0.1°C to 0.5°C (January and December) at Bahir Dar station. SDSM overestimated 0.1°C to 0.4°C thought the year and 0.1°C (at May) at Gondar station. The daily mean minimum temperature ranges from 6°C to 15.3°C at Bahir Dar and 8°C to 15.1°C at Gondar station.

5.2.3. Comparison of RCM and SDSM simulated against observed precipitation

Figure 17 shows the mean monthly precipitation downscaled and RCM bias corrected in comparison with observed data for the baseline period (1981-2010). The SDSM and RCM model output performs reasonably well simulation of the mean monthly precipitation in most months though there is a relatively insignificant model error. Both at Bahir Dar and Gondar stations RCM-A1B shows overestimation ranging from 1 mm to 13 mm at months for November to April and underestimation ranging from 1mm to 15 mm for the months of May to September.

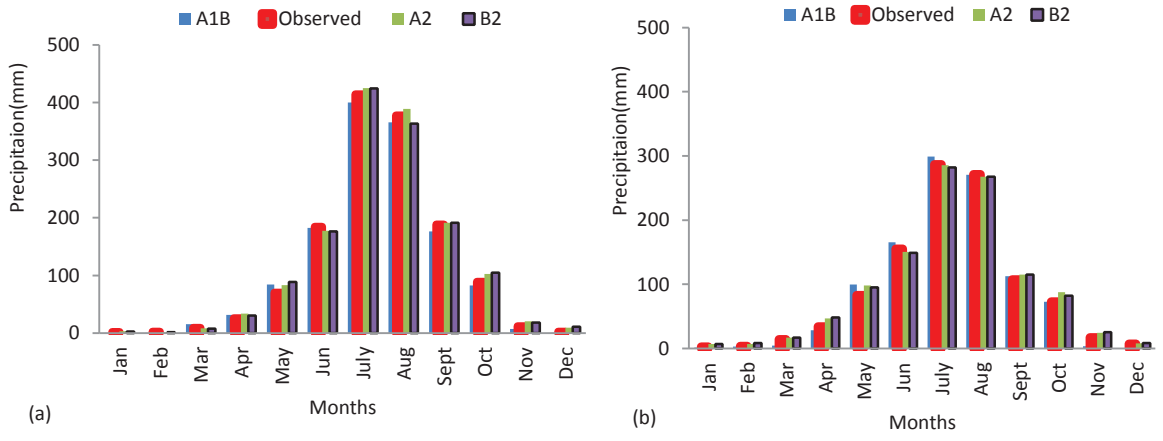

Figure 17: Mean monthly precipitation (1981-2010) of Bahir Dar (a) and Gondar (b) station

A2 and B2 shows underestimation of 1mm to 18 mm at month of September to May and overestimation of 1mm to 14 mm at months of June to August. In fact, precipitation downscaling is more difficult than temperature, because regional-scale predictors resolve daily precipitation amounts in a relatively poor manner depending on individual sites. According to (WCRP,2012), minor differences of the order of 20% are to be anticipated, however large differences are cause for some concern like weakness of downscaling method to capture regional climate dynamics aspect. In this case, this result can be taken as satisfactory. Observed and modelled result indicates that the total observed mean monthly precipitation in July is 414mm at Bahir Dar and 299mm at Gondar stations.

5.3. Projected change of climate variable statistics

The term anomaly means a devation of future climate condition from a baseline period (1981-2010) climate condition. In this study baseline period climatic condition is analysed based on meteorological station records of the study area. Positive anomaly indicates an increases from the baseline period value, while a negative anomaly indicates decrease from the baselin period value. The anomaly of monthly precipitation is calculated as the difference from future monthly average precipitation to the baseline period (1981-2010) monthly average precipitation values. The temprature is also calculated in the same way precipitation is calcualted.

HadCM3 predictor variables in the two given climate change scenarios (A2 and B2) were employed in SDSM downscaling processes to generate temperature and precipitation scenarios of the three future time windows, namely 2011-2040(2020s), 2041-2070(2050s) and the 2071-2099(2080s). In the same way RCM model scenario (A1B) were also analysed. Respective results of precipitation, maximum and minimum temperature of each scenario are discussed in section 5.2.1-5.2.3.

5.3.1. Projected changes in monthly rainfall statistics

Projected changes in monthly rainfall statistics are vital means of evaluating the characteristics of rainfall at the study site. Figure 18 shows the general pattern of the change anomalies in monthly precipitation against the observed baseline period (1981-2010) at Bahir Dar station. Anomalies were calculated as the difference from observed baseline period average precipitation to future periodic monthly average precipitation value.

The A2 and B2 scenario noted an overall increasing pattern in the monthly precipitation particularly in August-November (28-60mm) and April-May (4.7-8.7mm), while a consistently decreasing pattern is showed for the months of June-July (25- 50mm). For the months of December–March no change was observed for all future windows. The RCM A1B scenario show an overall decreasing pattern in the monthly precipitation particularly in the month of May–August (1.7-57.8mm at 2020s), (9.4-90.1mm at 2050s) and (1-193.8mm at 2080s). The consistent increasing pattern is revealed in the month of September – October (7.6-12.0mm at 2020s), (28.3-34.3mm at 2050s) and (1.3-14.3mm at 2080s). The rest of months showed a similar pattern with the baseline period.

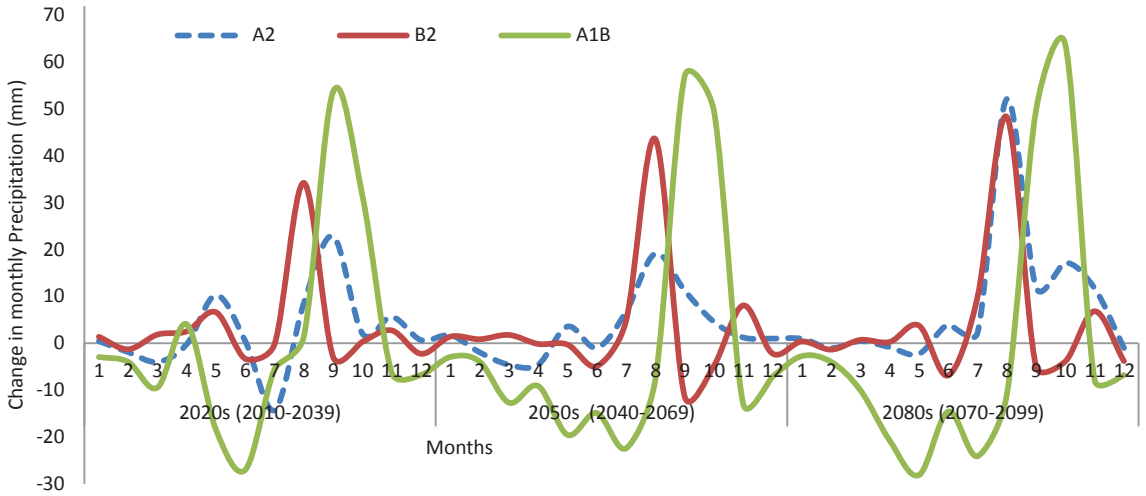

Figure 18: Change anomalies of monthly precipitation for future windows at Bahir Dar station

5.3.2. Projected changes in maximum temperature statistics

Figure 19 shows the change anomalies in mean monthly maximum temperature of A1B (RCM), A2 (SDSM) and B2 (SDSM) scenarios for future periods. The A1B scenario simulation indicates an overall increasing pattern of + 0.1 to +0.7°C at 2020s,+0.2 to 2.4°C at 2050s and +1.1 to +3.6°C at the end of 21st century. The A2 scenario shows increases of +0.1 to + 0.4°C at 2020s, +0.3 to +1.5°C at 2050s and +1.6 to +3.0°C at 2080s. B2 scenario shows increasing pattern from +0.1 to 0.5°C at 2020s, +0.7 to +1.3°C at 2050s and +0.8 to +2.3°C the end of 21st century. The B2 and A2 scenarios show identical pattern with A2 but large differences in temperature changes was noted from 2050s period and onwards. In general the three scenarios A1B, A2 and B2 shows increasing pattern of mean monthly maximum temperature.

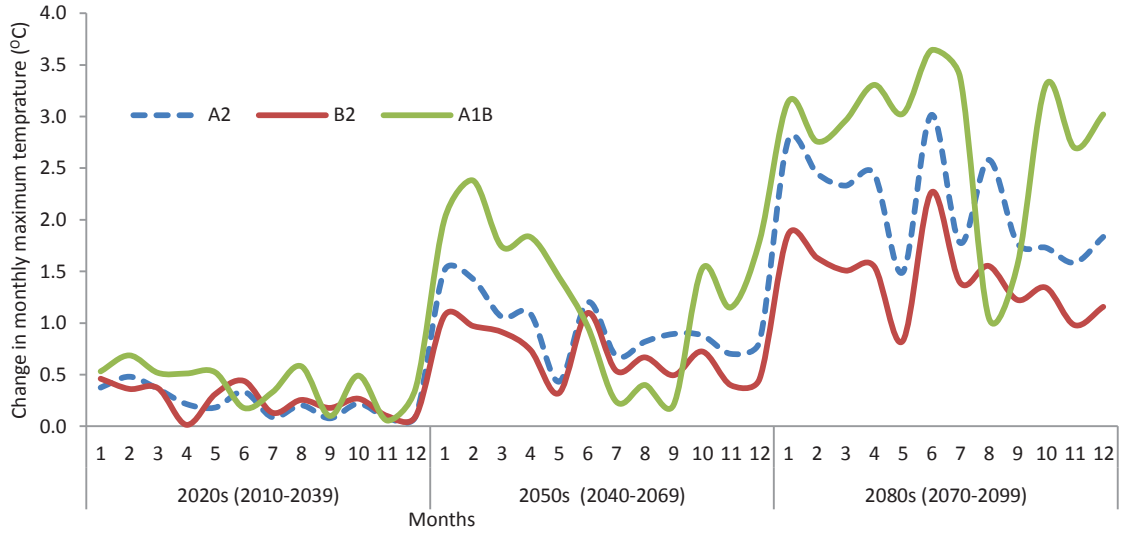

Figure 19: Change anomalies of monthly maximum temperature for future windows as Bahir Dar station

5.3.3. Projected changes in minimum temperature statistics

Figure 20 shows the change anomalies in mean monthly minimum temperature of A1B (RCM), A2 (SDSM) and B2 (SDSM) scenarios for future periods. The A1B scenario simulation indicates an overall

increasing pattern of +0.3 to +0.7°C at 2020s, +0.1 to +1.7°C at 2050s and +0.1 to +2.7°C at the end of 21st century except normal pattern at the month July and November in 2020s.
Both A2 and B2 scenarios noted consistent increases. The A2 scenario showed increase of +0.1 to +1.1 °C in the 2020s, +0.1 to +2.3°C in the 2050s and +0.8 to +3.9°C in the 2080s. B2 scenario shows increase from +0.1 to +0.8°C at 2020s, +0.9 to +1.7°C at 2050s and +0.1 to 2.7°C at the end of 21st century. In general the three scenarios A1B, A2 and B2 shows increasing pattern of mean monthly minimum temperature.

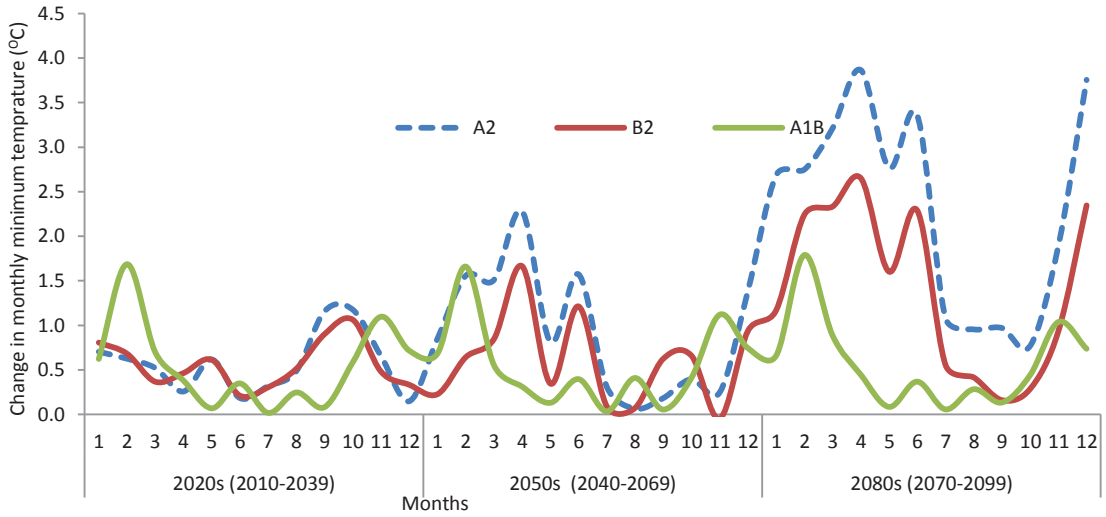

Figure 20: Change anomalies of monthly minimum temperature for future windows at Bahir Dar station

5.4. Lake Water Balance components

5.4.1. Lake evaporation

Over Lake Precipitation is one of the major components of the lake water balance and it is estimated based on inverse distance weighting method using five stations (Figure 10) around the lake. The weight of each station in the Lake Tana basin is calculated by inverse distance weighting method, which is presented in Table 10. A detailed description of inverse distance weighting method is presented in section 4.5.1). All stations are relatively in close proximity to the lake with adequate data for downscaling of precipitation.

Table 10: Weight of stations used to estimate lake precipitation and evaporation

Station	Adet	Bahir Dar	Debra Tabor	Dangila	Gondar
Weight	0.15	0.33	0.16	0.07	0.29

Annual mean lake evaporation at 2020s, 2050s and 2080s is 2097mm, 2107 and 2120mm respectively.
Figure 21 shows the annual mean lake evaporation for A2 scenario of the three future windows ranging from 2090 mm (lowest at 2020s) to 2134mm (highest at end of 21st century). Annual mean lake evaporation at 2020s, 2050s and 2080s is 2097mm, 2107 and 2120mm respectively. It indicates overall increasing pattern of mean annual lake evaporation in comparison to the reference period evaporation.

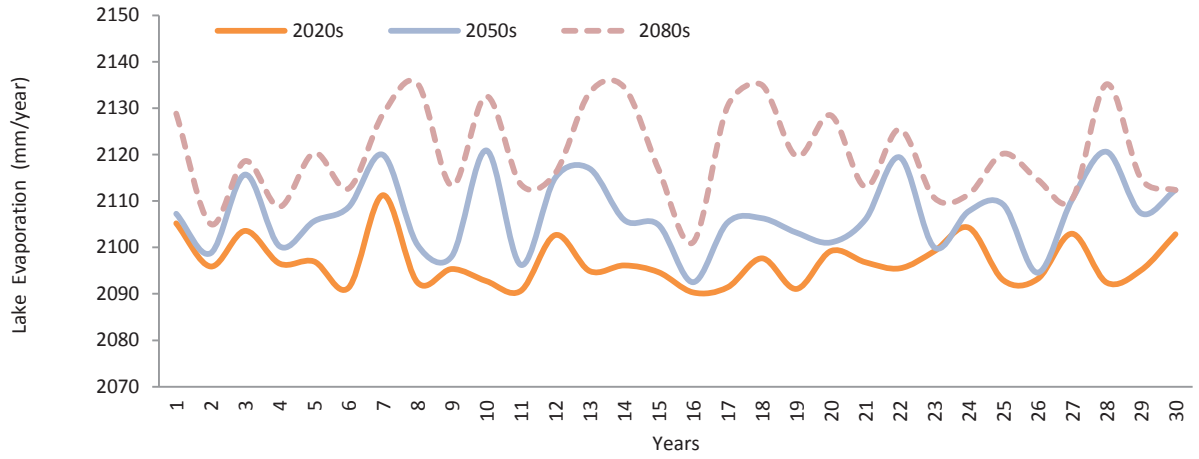

Figure 21: Over-lake annual evaporation of A2 scenario output

Figure 22 shows the annual mean lake evaporation for B2 scenario of the three future windows ranging from 1987 mm (lowest at 2020s) to 2263mm (highest at end of 21st century). Annual mean lake evaporation at 2020s, 2050s and 2080s is 2098mm, 2107 and 2118mm respectively. It shows overall increasing pattern when compared to the reference period evaporation and inter-annual variability of the model outputs.

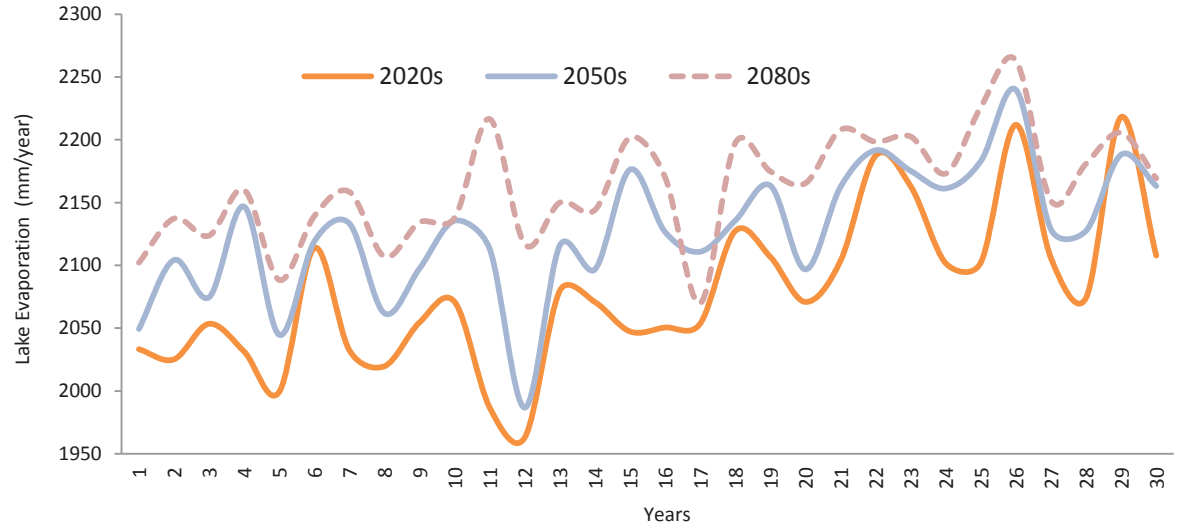

Figure 22: Over-lake annual evaporation of B2 scenario output

Figure 23 shows the annual mean lake evaporation for A1B scenario of the three future windows ranging from 1963 mm (lowest at 2020s) to 2263mm (highest at the end of 21st century). Annual mean lake evaporation at 2020s, 2050s and 2080s is 2079mm, 2127 and 2162mm respectively. It shows overall increasing pattern when compared to the reference period evaporation and inter-annual variability shows the sensible representation of nature by the model outputs.

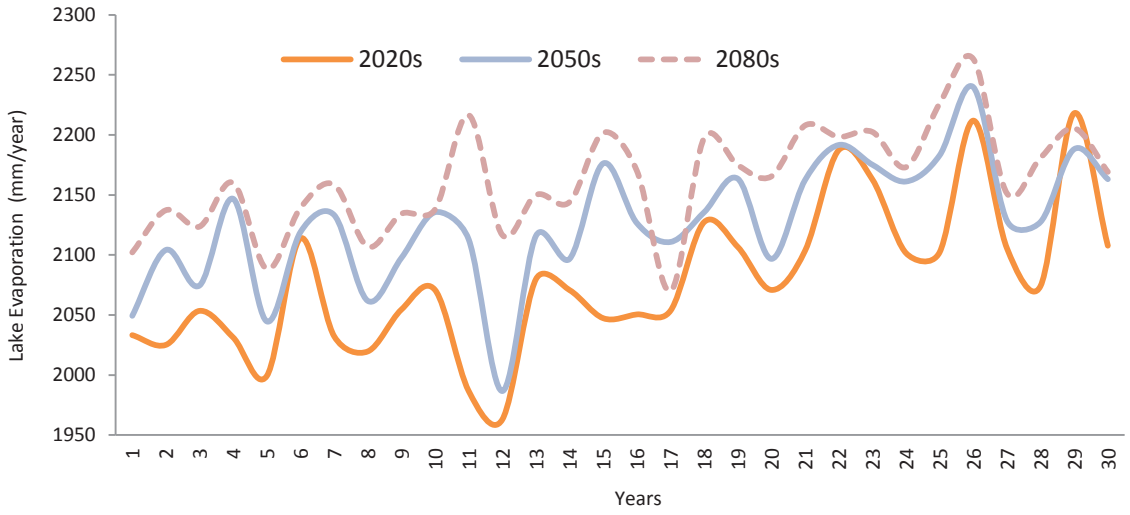

Figure 23: Over-lake annual evaporation of A1B scenario output

In general the increase of lake evaporation is due to increase of maximum and minimum temprature for all the three scenarios (i.e A1B, A2 and b2) as indicated on appendex E.

5.4.2. Lake precipitation

Over Lake Precipitation is one of the major components of the lake water balance and it is estimated based on inverse distance weighting method using five stations (see Figure 10) around the lake. A detailed description of interpolation of rainfall is presented in (section 4.5.1). All stations are relatively in close proximity to the lake with adequate data for downscaling of precipitation.

SDSM output A2 emission scenario estimate shows the future mean annual precipitation each time horizons is highly variable and irratic. As indicated in Figure 24, projection of A2 scenario annual over-lake precipitation did not shows a systematic increase or decreas in all future time horizons. In most of the yaers at each future windows A2 scenario shows increase of annual lake precipitation of 1-6%, 1-5% and 1-7% for the 2020s, 2050s and 2080s and incontarary some of the years shows decrease of 1-5% at 2020s, 1-3% at 2050s respective future windows by when compared to the baseline period.. The general pattern shows consistent increase of mean annual over-lake precipitation at the end of 21st century.

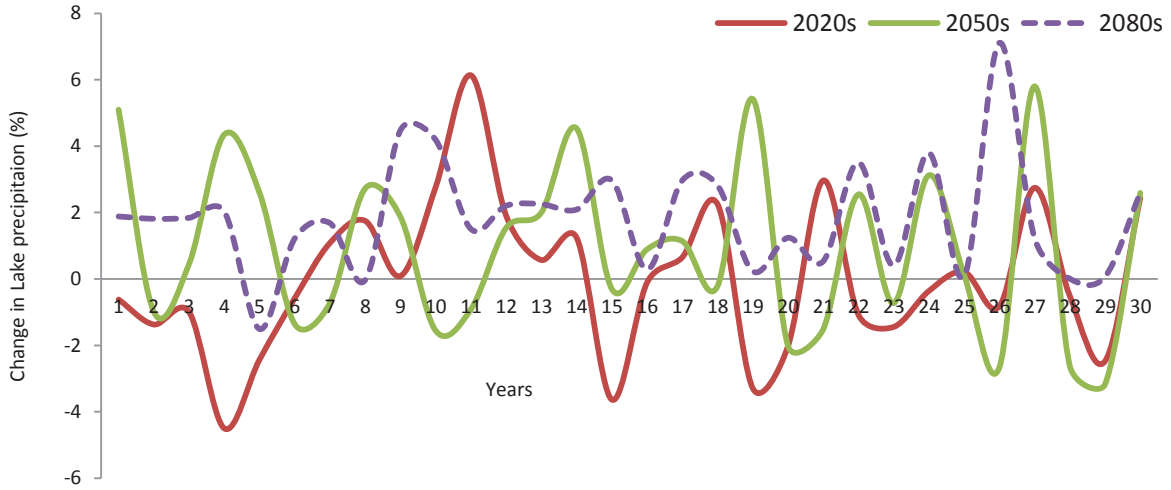

Figure 24: Pattern of the change anomalies of annual precipitation of Lake Tana for A2 scenario output

Downscaled B2 scenario output of the lake precipitation estimation in Figure 25 shows increase of annual over-lake precipitation in most of the years by 1-4.2%, 1-4% and 1-8.4% for the 2020s, 2050s and 2080s respective future windows by as compared to the baseline period. In contrary it also noted that decrease in few years by 1-4% at beginning and end of 2020s, 1-4.4% at beginning and end of at 2050s, 1-2% at beginning and 5% at end of 21st century. The overall pattern shows consistent increase of mean annual Over-lake precipitation at the end of 21st century.

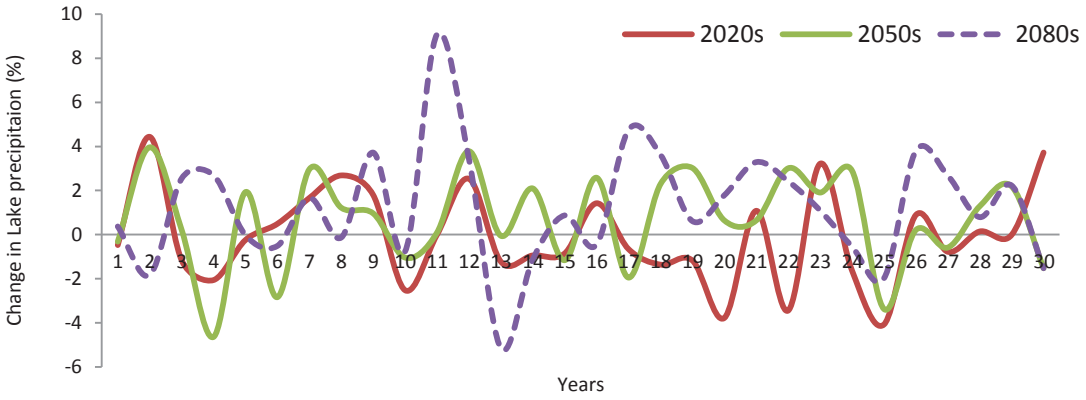

Figure 25: Pattern of the change anomalies of annual precipitation of Lake Tana for B2 scenario output

Downscaled A1B scenario output of the lake precipitation estimation (see Figure 26) shows increase of annual over-lake precipitation at the beginning and decrease at the end of respective future windows. In most of the years of respective window over-lake precipitation increases 1-19% ,1-33%, 1-4% and 1-29% for the 2020s, 2050s and 2080s respective future windows when compared to the baseline period. In contrary it also noted that decrease in some years by 1-22% at 2020s, 1-29% at 2050s, 1-22% at end of 21st century. The overall pattern shows inconsistent increase of mean annual Over-lake precipitation 69% at 2020s and decrease by 10% at 2050s and by 11% at end of 21st century.

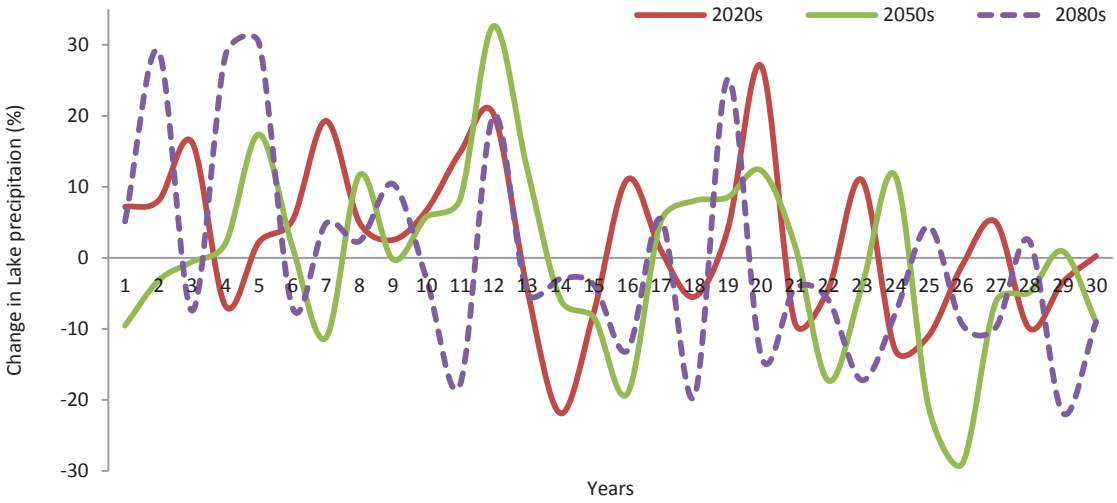

Figure 26: Pattern of the change anomalies of annual precipitation of Lake Tana for A1B scenario output

5.5. Inflows from Gauged and Ungauged

The total inflow to the lake is estimated from gauged and ungauged by summing the inflows from all catchments. The inflow from each catchment is simulated based on downscalled SDSM and RCM bias corrected data (i.e daily precipitation, mean temperature and evaporation) of stations arround the lake Tana. The unit of precipitation and the evaporation is mm/day, inflow from catchment which is simulated in m3/s multiplied by the factor 86.4 and divided by the area of catchment to convert m^3/s to mm/day to make units of water balance component the same.

Ungauged catchment model parameters can be determined in several ways; some of these are the multiple linear regression, spatial proximity and area ratio method. Multiple linear regression method is developed and recommended by (Perera,2009) for Lake Tana ungauged catchments and is adapted for this study. This method correlates physical catchment characteristic and calibrated model parameters of the gauged catchments that serve to estimate model parameters for the ungauged catchments.
The regional model adopted from (Perera (2009) see Table 11) was used to estimate the model parameters of ungauged catchment using their physical catchment characteristics (PCCs). The PCCs are listed for respective catchments in Appendix F.

Table 11: Statistical characteristics for the regression equation of model parameters modified after Perera (2009)

Model parameters	β_0	β_1	β_2	β_3
$ALFA = \beta_0 + \beta_1 \cdot AREA + \beta_2 \cdot URBAN$	0.45233	-0.00009	-0.7365	
$BETA = \beta_0 + \beta_1 \cdot SHAPE + \beta_2 \cdot HI$	7.511	-0.036	-8.544	
$CFLUX = \beta_0 + \beta_1 \cdot SHAPE + \beta_2 \cdot PDRY + \beta_3 \cdot PET$	-0.2184	-0.0082	0.3867	0.0007
$FC = \beta_0 + \beta_1 \cdot HI$	3520.82	-6651.21		
$KF = \beta_0 + \beta_1 \cdot SAAR$	-0.0656	0.00009		
$KS = \beta_0 + \beta_1 \cdot AVGSLOPE$	0.0187	0.0018		
$LP = \beta_0 + \beta_1 \cdot HI + \beta_2 \cdot LUV$	-2.2435	5.8697	0.0027	
$PERC = \beta_0 + \beta_1 \cdot DD + \beta_2 \cdot SAAR$	7.4926	0.0128	0.0005	

Statistical characteristics for the regression equation of model parameters that used to get calibrated model parameters for each catchment were presented in Table 12 above. Physical catchments characteristics and model parameters of gauged catchments used estimate model parameters of ungauged catchments are shown in Appendix F.

Table 12: Established model parameters of the ungauged catchments by the regional model.

	Ribb	Garno	Gilgal Abay	Gumera	Gelda	Megech	Gumero	Dema	Gabi Kura	Tana west
FC	461	461	794	328	395	461	395	262	328	262
BETA	2.46	1.30	3.29	2.81	2.26	1.90	1.82	1.85	2.62	2.53
LP	0.52	0.46	0.31	0.72	0.78	0.49	0.54	0.65	0.59	0.72
ALFA	0.37	0.38	0.18	0.41	0.17	0.39	0.39	0.41	0.40	0.39
KF	0.04	0.02	0.07	0.06	0.06	0.04	0.04	0.04	0.02	0.01
KS	0.06	0.08	0.05	0.05	0.05	0.05	0.07	0.02	0.05	0.06
PERC	0.98	2.54	1.77	1.94	2.23	1.06	1.87	1.84	2.46	2.40

CFLUX	0.77	0.56	1.00	0.99	0.94	0.72	0.68	0.83	0.96	0.87

5.5.1. Gauged catchments surface water inflow

As shown in Figure 27 projection of A1b scenario annual surafe water inflow shows a systematic decreas in all future time horizons. In most of the years at each future windows A1B scenario shows decrease of annual surafe water inflow of 1-47%, 1-49% and 1-69% for the 2020s, 2050s and 2080s and incontarary some of the years shows the increase of 1-45% at 2020s and 2050s future windows when it is compared to the baseline period.. In general consistent decrease of mean annual surafe water inflow at the end of 21st century.

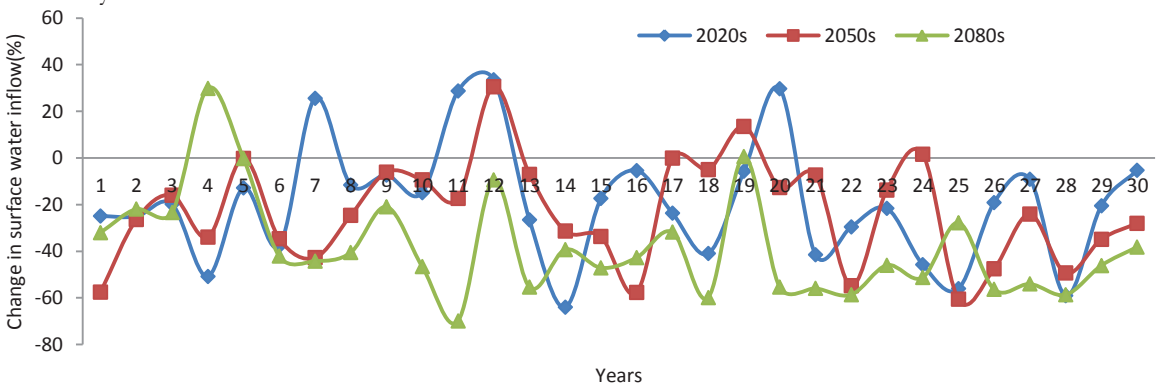

Figure 27: Pattern of the change anomalies of annual gauged catchments surface water inflow of Lake Tana for A1B scenario output

SDSM output A2 emission scenario based estimateion of mean annual surface water inflows of the Lake from guaged catchments each time horizons shows is highly inter-annual variablity and irratic charcaterists. Figure 28 shows projected A2 scenario annual surafe water inflow systematic increas in all future time horizons. In general A2 scenario shows increase of annual surafe water inflow of 17-23%, 18-28% and 19-28% for the 2020s, 2050s and 2080s.

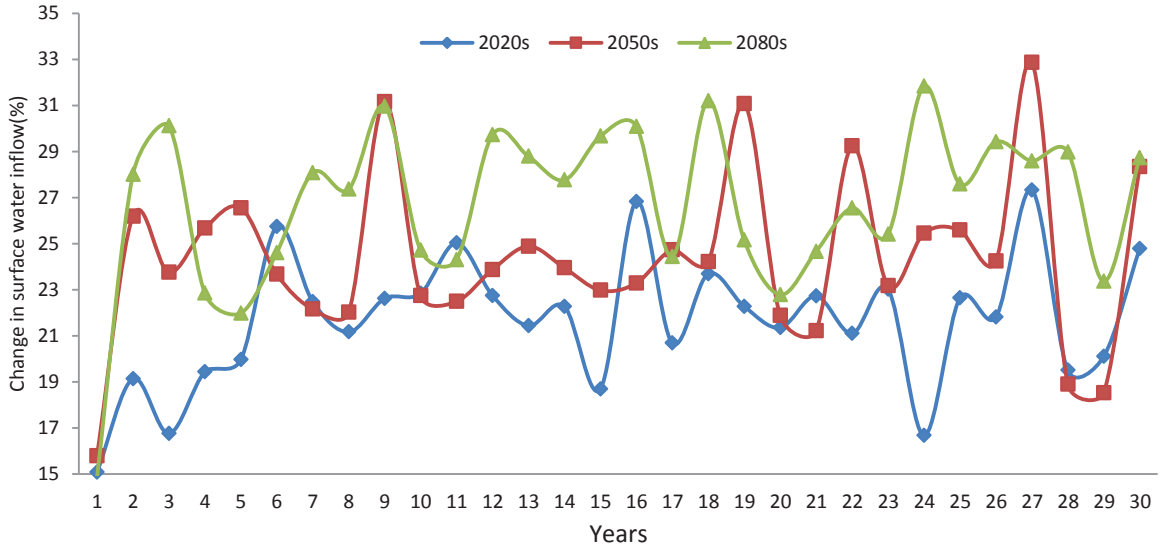

Figure 28: Pattern of the change anomalies of annual gauged catchments surface water inflow of Lake Tana for A2 scenario output

Figure 29 shows projected B2 scenario annual surafe water inflow systematic increas in all future time horizons. In general A2 scenario shows increase of annual surafe water inflow of 11-24%, 12-28% and 10-31% for the 2020s, 2050s and 2080s.

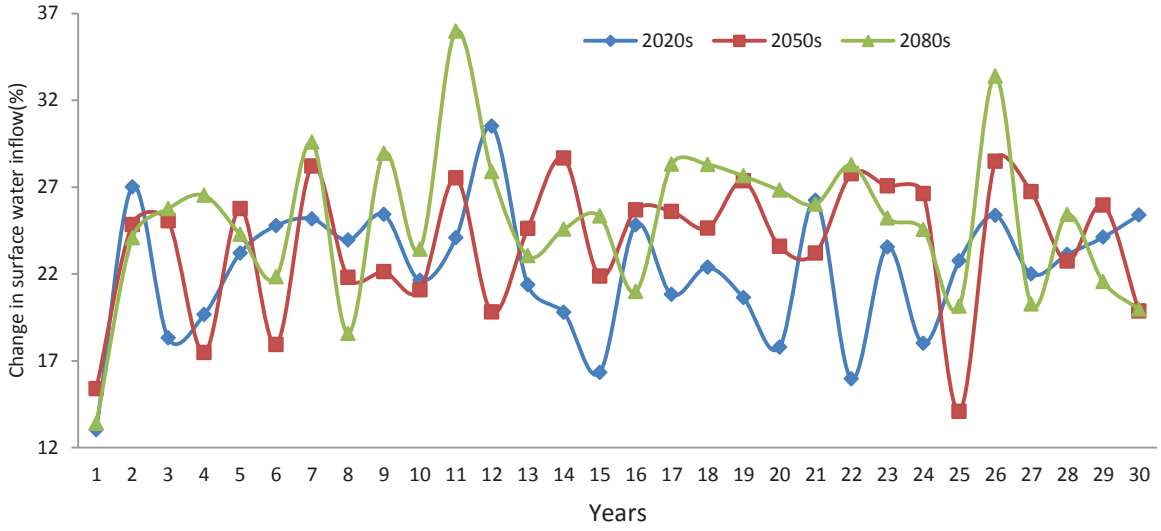

Figure 29: Pattern of the change anomalies of annual gauged catchments surface water inflow of Lake Tana for B2 scenario output

In general, both A2 and B2 based estimation of surface water inflows from gauged catchments shows generally increasing pattern while A1B shows decreasing pattern for all future windows.

5.5.2. Ungauged catchments surface water inflow

As noted in Figure 29 projected A1B scenario annual surafe water inflow from unguaged catchments shows a systematic decreas in all future time horizons except some years in 2020s and 2050s. In most of the years for respective windows A1B scenario shows decrease of annual surafe water inflow 1-47%, 1-52% and 1-71% for the 2020s, 2050s and 2080s respectively; incontarary some of the years shows the increase of 1-55% at 2020s and 1-51% at 2050s when it is compared to the baseline period.. In general consistent decrease of mean annual surafe water inflow from unguaged catchments likely expected at the end of 21st century.

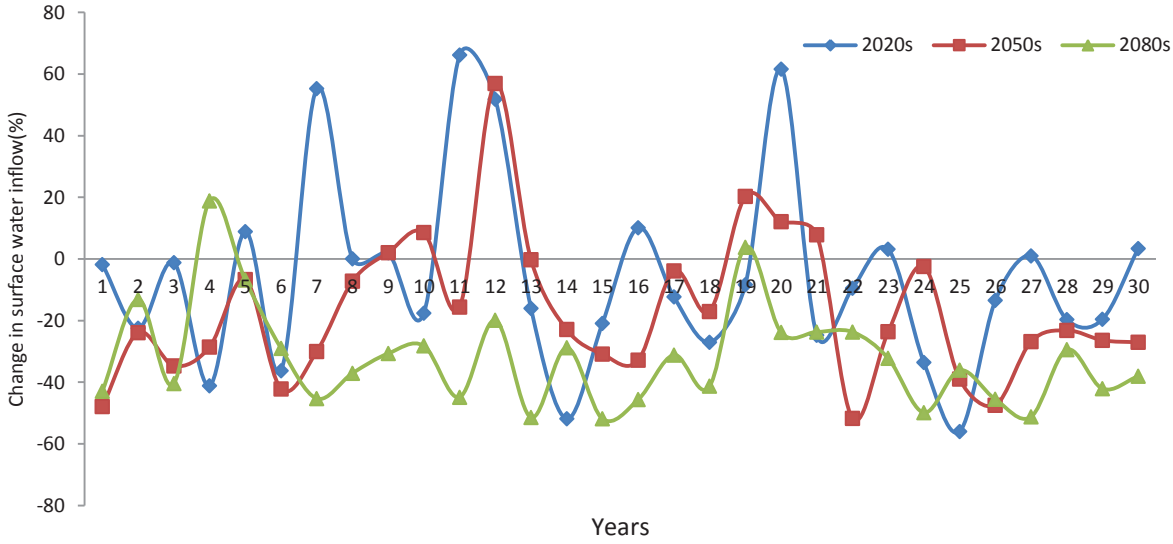

Figure 30: Pattern of the change anomalies of annual ungauged catchments surface water inflow of Lake Tana for A1B scenario output

Figure 31 shows projected A2 scenario annual surafe water inflow from unguaged catchments that noted systematic increas in all future time horizons. In general A2 scenario based annual surafe water inflow from ungauged catchments shows increase of 5-26%, 12-30% and 14-28% for the 2020s, 2050s and 2080s respectively.

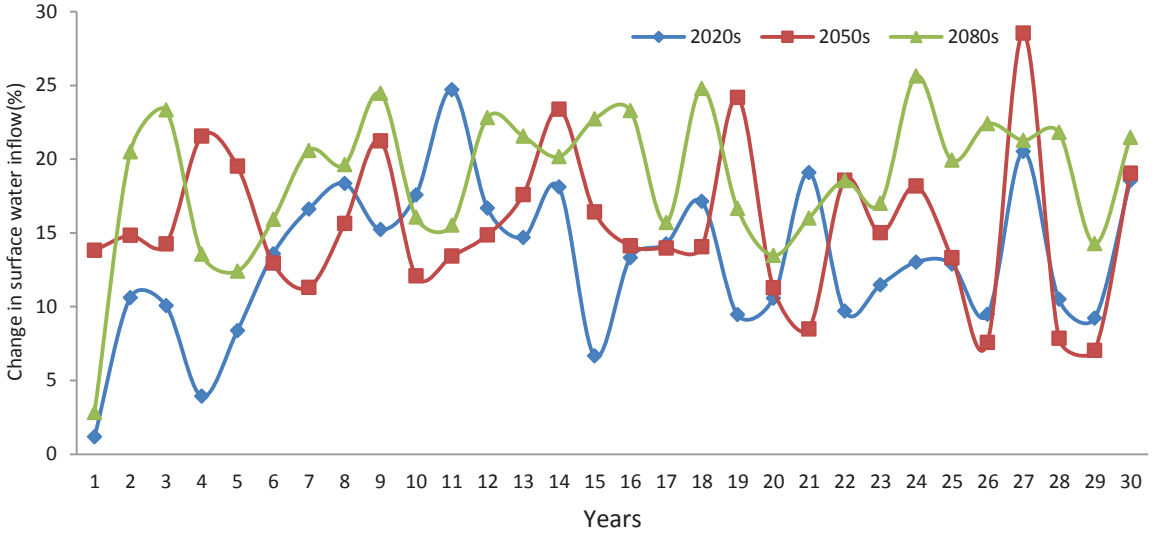

Figure 31: Pattern of the change anomalies of annual ungauged catchments surface water inflow of Lake Tana for A2 scenario output

Figure 32 shows projected B2 scenario annual surafce water inflow from unguaged catchments that noted systematic increas in all future time horizons. In general A2 scenario annual surafe water inflow from ungauged catchments noted an increase of 9-25%, 9-25% and 9-32% for the 2020s, 2050s and 2080s respectively.

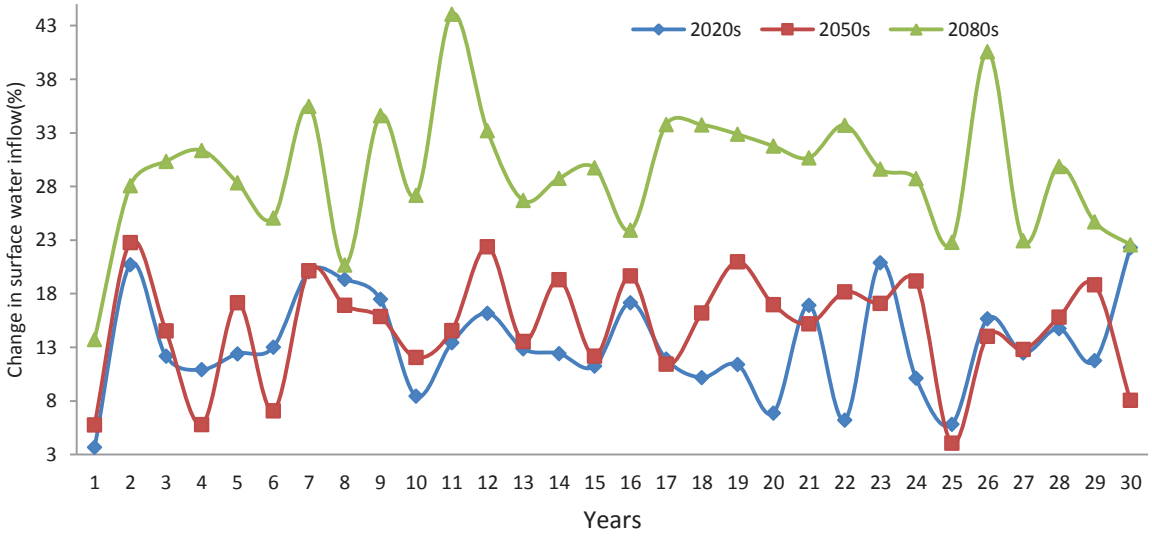

Figure 32: Pattern of the change anomalies of annual ungauged catchments surface water inflow of Lake Tana for B2 scenario output

In general, both A2 and B2 based estimation of surface water inflows from ungauged catchments shows generally increasing pattern while A1B shows decreasing pattern for all future windows.

5.6. Projected Lake water balance Analysis

Table 13 shows summary of water balance components with expected percentage changes. The water balance is estimated based on the inflow and the outflow of the Lake Tana. The inflow component is the summation of the over-lake precipitation and stream flow from gauged and ungauged rivers. The outflow component is the summation of the over-lake evaporation and outflow from the lake through the Blue Nile River.

In this study, lake water balance is established for the baseline period (1981-2010) and the three future time horizons 2020s, 2050s and 2080s. The sum of the inflow from 9 gauged and 10 ungauged catchments is used to estimate the total stream flow into the lake. Stream flow for the future time horizons is simulated using the downscaled rainfall, mean temperature, reference evaporation and calibrated model parameters.

Table 13: Water Balance components (mm/year) with expected percentage changes (%)

LWB components	Baseline	Scenarios	2020s	2050s	2080s
Gauge catchment Surface water inflow	1253	A1B	+1011(-19%)	+964(-23%)	+775(-38%)
		A2	+1524(+22%)	+1558(+24%)	+1588(+27%)
		B2	+1531(+22%)	+1550(+24%)	+1566(+25%)
Ungauged catchment Surface water inflows	933	A1B	+880(-6%)	+776(-17%)	+634(-32%)
		A2	+1056(+13%)	+1077(+15%)	+1108(+19%)
		B2	+1057(+13%)	+1072(+15%)	+1206(+29%)
Over lake Rainfall	1274	A1B	+1215(-5%)	+1118(-12%)	+938(-26%)
		A2	+1386(+9%0	+1399(+10%)	+1411(+11%)
		A2B	+1385(+9%)	+1396(+10%)	+1404(+10%)
Over-lake Evaporation	2041	A1B	-2079(+2%)	-2127(+4%)	-2162(+6%)
		A2	-2097(+3%0	-2107(+3%)	-2120(+4%)
		A2	-2098(+3%)	-2107(+3%)	-2118(+4%)
Lake outflow (BNR)	1520		-1520(0%)	-1520(0%)	-1520 (0%)
Storage change	-101	A1B	-493	-789	-1335
		A2	+349	+407	+467
		B2	+355	+390	+537

Values in (+) indicates increase and (–) decreases of change in percentage.

In general, result of SDSM for A2 and B2 emission scenario sows increasing pattern of inflows to the lake, over-lake precipitation and evaporation. In contrary, A1B scenario indicates a decrease of inflow component such as over-lake precipitation and surface water inflow, meanwhile an increase of over-lake evaporation for future windows shown. The decreasing pattern of the A1B scenario for precipitation and surface runoff shows agreement with previous study of Taye et al. (2011) on the Blue Nile region.

6. CONCLUSIONS AND RECOMMENDATIONS

Understanding the water balance components of Lake Tana is vital to develop forward-looking and science-based management plans in current and future dynamic and changing climatic conditions. In this study hydrological impact of climate change on Lake Tana water balance components were evaluated in response to the A1B, A2 and B2 emission scenarios. The Statistical Downscaling Model (SDSM 4.2 version) was used to downscale finer and reliable estimate of climatic variables using predictors obtained from the HadCM3 experiment for both A2 and B2 Scenario. The Regional Climate Model (RCM) output for A1B scenario analysed based on ground control point results of CCLM. Hydrological model (HBV) was used to simulate surface water inflow.

Hydrological impact of climate change between baseline period and future time windows lake water balance was investigated using three climate scenarios. Based on the result of these three scenarios (i.e. A1B, A2 and B2) conclusion and recommendation of this study are presented as follows.

6.1. Conclusions

SDSM scenarios (i.e. A2 and B2) and RCM output scenario (i.e. A1B) minimum temperature show an increasing pattern in all future time horizons. The A1B scenario monthly maximum simulation indicates an overall increasing pattern of +0.1 to +0.7°C at 2020s, +0.2 to 2.4°C at 2050s and +1.1 to +3.6°C at the end of 21st century. The A2 of SDSM scenario shows increases of +0.1 to +0.4°C at 2020s, +0.3 to +1.5°C at 2050s and +1.6 to +3.0°C at 2080s. B2 scenario of SDSM shows increasing pattern from +0.1 to 0.5°C at 2020s, +0.7 to +1.3°C at 2050s and +0.8 to +2.3°C the end of 21st century. The B2 scenarios show identical increasing pattern with A2 but large differences in temperature changes was noted from 2050s period and onwards.

The A2 , B2 scenarios and A1B scenario minimum temprature noted consistent increases. The A2 scenario showed increase of +0.1 to +1.1°C in the 2020s, +0.1 to +2.3°C in the 2050s and +0.8 to +3.9°C in the 2080s. B2 scenario shows increase from +0.1 to +0.8°C at 2020s, +0.9 to +1.7°C at 2050s and +0.1 to 2.7°C at the end of 21st century. The A1B scenario simulation indicates an overall increasing pattern of +0.3 to +0.7°C at 2020s, +0.1 to +1.7°C at 2050s and +0.1 to +2.7°C at the end of 21st century except normal pattern at the month July and November in 2020s.

Contrary to the temperature, for the three scenarios does not shows a systematic increase or decrease in all future time horizons of precipitation. The A2 and B2 scenario noted an overall increasing pattern in the monthly precipitation particularly in August-November (28-60mm) and April-May (4.7-8.7mm), while a consistently decreasing pattern is showed for the months of June-July (25-50mm). The A1B scenario noted an overall decreasing pattern in the monthly precipitation particularly in the month of May-August (1.7-57.8mm at 2020s), (9.4-90.1mm at 2050s) and (1-193.8mm at 2080s); but consistent increasing pattern is also revealed in the month of September-October (7.6-12.0mm at 2020s), (28.3-34.3mm at 2050s) and (1.3-14.3mm at 2080s).

The water balance components of the Lake Tana for the future time is computed based on the lake precipitation, the lake evaporation, the inflow to the lake and the lake outflow through Blue Nile River. In general, A2 and B2 scenarios of SDSM shows increasing pattern of inflows to the lake, over-lake precipitation and evaporation. A1B scenario indicates the decrease of inflow component such as over-lake precipitation and surface water inflow while increase of over-lake evaporation for future windows. Decreasing pattern of A1B scenario for precipitation and surface runoff shows agreement with study of Taye et al. (2011) on Blue Nile region.

6.2. Recommendation

The climate models SDSM, RCM and their outputs for temperature and precipitation are used in this study where the models and their output are possessed a certain level of uncertainty. Consequently, the methods applied for this study should be used to provide an indication to the likely hydrological impact of climate change on Lake Tana water balance.

Three emission scenarios are applied in this study but in the actual case according (Ward et al.,2011) "all SRES emission scenarios have equal probability of occurrence". Therefore, the results of this study should be considered as indicative of the likely future and interpretation should be done with care. This study gives evidence and increase awareness on the possible future impacts of climate change on Lake Tana water balance. The future studies should also consider the entire range of possible emission scenarios and more models.

LIST OF REFERANCES

Abdo, K. S., Fiseha, B. M., Rientjes, T. H. M., Gieske, A. S. M., & Haile, A. T. (2009). Assessment of climate change impacts on the hydrology of Gilgel Abay catchment in Lake Tana basin, Ethiopia. [Article]. *Hydrological Processes, 23*(26), 3661-3669.

Afifi, A. A., & Clark, V. (1996). Computer-Aided Multivariate Analysis. Third Edition. Chapman & Hall. *Biometrical Journal, 39*(7), 875-876. doi: 10.1002/bimj.4710390716

Akhtar, M., Ahmad, N., & Booij, M. J. (2008). The impact of climate change on the water resources of Hindukush-Karakorum-Himalaya region under different glacier coverage scenarios. *Journal of Hydrology, 355*(1-4), 148-163. doi: 10.1016/j.jhydrol.2008.03.015

Bekele, H. M. (2009). *Evaluation of Climate Change Impact on Upper Blue Nile Basin Reservoirs (Case Study on Gilgel Abay Reservoir, Ethiopia)* Arba Minch University (School of Post Graduate Studies), Arbaminch.

Berg, P., Feldmann, H., & Panitz, H. J. (2012). Bias correction of high resolution regional climate model data. [Article]. *Journal of Hydrology, 448*, 80-92. doi: 10.1016/j.jhydrol.2012.04.026

Beyene, T., Lettenmaier, D. P., & Kabat, P. (2010). Hydrologic impacts of climate change on the Nile River Basin: implications of the 2007 IPCC scenarios. *Climatic Change, 100*(3-4), 433-461.

Booij, M. J. (2005). Impact of climate change on river flooding assessed with different spatial model resolutions. *Journal of Hydrology, 303*(1-4), 176-198. doi: 10.1016/j.jhydrol.2004.07.013

Burger, M., C., Kolditz, O., Fowler, H. J., & Blenkinsop, S. (2007). Future climate scenarios and rainfall-runoff modelling in the Upper Gallego catchment (Spain). *Environmental Pollution, 148*(3), 842-854.

Canada, E. (2012 April 19, 2012). Regional Climate Models, from http://www.cccsn.ec.gc.ca/?page=rcm

Carrillo , G. F. M., Gonzalez, R. M. E., Cornejo, L. V. M., Martinez, H. V., Zaragoza, V. F., & Navarro, R. M. D. (2008). Evaluation of the evapotranspiration in the Chapala Lake using weather and remote sensing data. In K. Oleschko, S. Cherkasov, J. L. PalacioPrieto, V. TorresArguelles, C. I. GaonaSalado, A. G. CastanedaMiranda & S. A. ZamoraCastro (Eds.), *Gis in Geology and Earth Sciences* (Vol. 1009, pp. 169-179). Melville: Amer Inst Physics.

Carter, T. R. (2007). General Guidelines on the use of scenario data for Climate Impact and Adaptation Assessment. doi: Finnish Environmental Institute, Helsinki, Finland

Chebud, Y. A., & Melesse, A. M. (2009). Modelling lake stage and water balance of Lake Tana, Ethiopia. *Hydrological Processes, 23*(25), 3534-3544. doi: 10.1002/hyp.7416

Climate-decisions.org. (2008, July 25,2012). Downscaling Climate Data, from http://www.climate-decisions.org/2_Downscaling%20Climate%20Data.htm

Dickinson, R. E., Errico, R. M., Giorgi, F., & Bates, G. T. (1989). A REGIONAL CLIMATE MODEL FOR THE WESTERN UNITED-STATES. *Climatic Change, 15*(3), 383-422.

Elshamy, M. E., Sayed, M. A.-A., & Badawy, B. (2009). Impacts of Climate Change on the Nile Flows at Dongola Using Statistical Downscaled GCM Scenarios *Nile Basin Water Engineering Scientific Magazine, 2*.

FAO. (2012). FAO Penman-Monteith equation Retrieved February 01 2013, from http://www.fao.org/docrep/X0490E/x0490e06.htm

Gagnon, S., Singh, B., Rousselle, J., & Roy, L. (2005). An Application of the Statistical DownScaling Model (SDSM) to Simulate Climatic Data for Streamflow Modelling in Québec. *Canadian Water Resources Journal, 30*(4), 297-314. doi: 10.4296/cwrj3004297

Giorgi, F., Marinucci, M. R., & Visconti, G. (1990). USE OF A LIMITED-AREA MODEL NESTED IN A GENERAL-CIRCULATION MODEL FOR REGIONAL CLIMATE SIMULATION OVER EUROPE. *Journal of Geophysical Research-Atmospheres, 95*(D11), 18413-18431.

Gordon, C., Cooper, C., Senior, C. A., Banks, H., Gregory, J. M., Johns, T. C., . . . Wood, R. A. (2000). The simulation of SST, sea ice extents and ocean heat transports in a version of the Hadley Centre coupled model without flux adjustments. *Climate Dynamics, 16*(2-3), 147-168. doi: 10.1007/s003820050010

GWPF. (2011). IPCC Introduces New 'Climate Change' Definition from http://thegwpf.org/science-news/4374-ipcc-introduces-new-climate-change-definition.html

Haile, A. T., Rientjes, T., Gieske, A., & Gebremichael, M. (2009). Rainfall Variability over Mountainous and Adjacent Lake Areas: The Case of Lake Tana Basin at the Source of the Blue Nile River. *Journal of Applied Meteorology and Climatology, 48*(8), 1696-1717. doi: 10.1175/2009jamc2092.1

Hargreaves, G. H., & Samani, Z. A. (1982). Estimating potential evapotranspiration. *Journal of the Irrigation & Drainage Division - ASCE, 108*(IR3), 225-230.

Hay, E., L., Wilby, L., R., Leavesley, & H., G. (2000). A comparison of delta change and downscaled GCM scenarios for three mountainous basins in the United States. *Journal of the American Water Resources Association, 36*(2), 387-397.

Hessami, M., Gachon, P., Ouarda, T. B. M. J., & St-Hilaire, A. (2008). Automated regression-based statistical downscaling tool. *Environmental Modelling & Software, 23*(6), 813-834. doi: http://dx.doi.org/10.1016/j.envsoft.2007.10.004

Houghton, J. T., Ding, Y., Griggs, D. J., Noguer, M., Linden, P. J. v. d., Dai, X., . . . Johnson, C. A. (2001). Climate change 2001: the scientific basis:contribution of working group I to the third assessment report of theintergovernmental panel on climate change..

Huang, J., Zhang, J. C., Zhang, Z. X., Sun, S. L., & Yao, J. (2012). Simulation of extreme precipitation indices in the Yangtze River basin by using statistical downscaling method (SDSM). *Theoretical and Applied Climatology, 108*(3-4), 325-343. doi: 10.1007/s00704-011-0536-3

Hulme, M., Doherty, R., Ngara, T., New, M., & Lister, D. (2001). African climate change: 1900-2100. *Climate Research, 17*(2), 145-168.

IPCC. (1994). IPCC Technical Guidelines for Assessing Climate Change Impacts and Adaptations.Prepared by Working Group II In T. R. Carter, M.L. Parry, H. Harasawa, and S. Nishioka and WMO/UNEP. CGER-IO15-'94 (Ed.). Tsukuba, Japan: University College - London, UK and Center for Global Environmental Research, National Institute for Environmental Studies.

IPCC. (2000). Special Report on Emissions Scenarios. In N. Nakicenovic & R. Swart (Eds.), *A Special Report of Working Group III of the Intergovernmental Panel on Climate Change*. Cambridge University Press, Cambridge, UK.

IPCC. (2007). Summary for Policymakers. In: Climate Change 2007: The Physical Science Basis. Contribution of Working Group I to the Fourth Assessment Report of the Intergovernmental Panel on Climate Change . . In S. Solomon, D. Qin, M. Manning, Z. Chen, M. Marquis, K.B. Averyt, M.Tignor and H.L. Miller (Ed.). Cambridge University Press,Cambridge,: United Kingdom and New York, NY, USA.

IPCC. (2012). IPCC Fourth Assessment Report: Climate Change 2007 (AR4) Retrieved May 30, 2012, from http://www.ipcc.ch/publications_and_data/ar4/syr/en/contents.html

Kibret, A. (2009). *Open water evaporation estimation using ground measurements and satellite remote sensing : a case study of lake Tana, Ethiopia.* ITC, Enschede. Retrieved from http://www.itc.nl/library/papers_2009/msc/wrem/kibret.pdf

Kim, U., & Kaluarachchi, J. J. (2009). Climate Change Impacts on Water Resources in the Upper Blue Nile River Basin, Ethiopia1. *Journal of the American Water Resources Association, 45*(6), 1361-1378. doi: 10.1111/j.1752-1688.2009.00369.x

Kling, Harald, Fuchs, Martin, Paulin, & Maria. (2012). Runoff conditions in the upper Danube basin under an ensemble of climate change scenarios. *Journal of Hydrology, 424-425*, 264-277.

Maidment, D. R. (2010). Handbook of Hydrology, from http://www.chipsbooks.com/hbhydrol.htm

Moss, R. H., Edmonds, J. A., Hibbard, K. A., Manning, M. R., Rose, S. K., van Vuuren, D. P., . . . Wilbanks, T. J. (2010). The next generation of scenarios for climate change research and assessment. [10.1038/nature08823]. *Nature, 463*(7282), 747-756.

NASA. (2010). Description of: Global Climate Change Key Indicators, from http://climate.nasa.gov/keyIndicators/

Nguyen, T.D., Nguyen, V. T. V., Gachon, P., & Bourque, A. (2004, June 16-18, 2004). *An Assessment of Statistical Downscaling Methods for Generating Daily Precipitation and Temperature Extremes in the Greater Montreal Region.* Paper presented at the 57th Annual Conference of the Canadian Water Resources Association, Montréal, QC.

Perera, U. J. B. (2009). *Ungauged catchment hydrology : the case of Lake Tana basin.* ITC, Enschede. Retrieved from http://www.itc.nl/library/papers_2009/msc/wrem/perera.pdf

Rientjes, T. H. M., Perera, B. U. J., Haile, A. T., Reggiani, P., & Muthuwatta, L. P. (2011a). Regionalisation for lake level simulation : the case of lake Tana in the upper blue Nile, Ethiopia. *Journal Hydrology and earth system sciences (HESS) : open access, 15*(4), 1167-1183.

Rientjes, T. H. M., Perera, J. B. U., Haile, A. T., & Gieske, A. S. M. (2011b). Hydrological balance of Lake Tana, upper Blue Nile basin, Ethiopia. *In: Nile River Basin : Hydrology, Climate and Water Use : e-book / editor A.M. Melesse. - Dordrecht : Springer, 2011. - 419 p. ISBN 978-94-007-0689-7. pp. 69-89.*

Seibert, J., & McDonnell, J. J. (2002). On the dialog between experimentalist and modeler in catchment hydrology: Use of soft data for multicriteria model calibration. *Water Resources Research, 38*(11). doi: 10.1029/2001wr000978

Setegn, S. G., Srinivasan, R., Melesse, A. M., & Dargahi, B. (2010). SWAT model application and prediction uncertainty analysis in the Lake Tana Basin, Ethiopia. *Hydrological Processes, 24*(3), 357-367. doi: 10.1002/hyp.7457

SMHI. (2006). The HBV model – its structure and applications. Retrieved August 24 2012, from http://www.smhi.se/en/Publications/hydrological-ensemble-forecasts-hydrologiska-ensembleprognoser-1.6763

Soliman, E. S. A., Sayed, M. A. A., & Jeuland, M. (2009). Impact Assessment of Future Climate Change for the Blue Nile Basin, Using a RCM Nested in a GCM. *Nile Basin Water Engineering Scientific Magazine, 2*.

Subramanya. (2008). *Engineering Hydrology*. 7 West Patel Nagar,New delhi 110 008: Tata McGraw-Hill.

Taye, M. T., Ntegeka, V., Ogiramoi, N. P., & Willems, P. (2011). Assessment of climate change impact on hydrological extremes in two source regions of the Nile River Basin. *Hydrol. Earth Syst. Sci., 15*(1), 209- 222. doi: 10.5194/hess-15-209-2011

Teutschbein, & Seibert. (2012). Bias correction of regional climate model simulations for hydrological climate-change impact studies: Review and evaluation of different methods. *Journal of Hydrology, 456–457*(0), 12-29. doi: http://dx.doi.org/10.1016/j.jhydrol.2012.05.052

Teutschbein, C., Wetterhall, F., & Seibert, J. (2011). Evaluation of different downscaling techniques for hydrological climate-change impact studies at the catchment scale. [Article]. *Climate Dynamics, 37*(9-10), 2087-2105. doi: 10.1007/s00382-010-0979-8

Vrac, M., Drobinski, P., Merlo, A., Herrmann, M., Lavaysse, C., Li, L., & Somot, S. (2012). Dynamical and statistical downscaling of the French Mediterranean climate: uncertainty assessment. *Natural Hazards and Earth System Sciences, 12*(9), 2769-2784. doi: 10.5194/nhess-12-2769-2012

Wale. (2008). *Hydrological balance of Lake Tana upper Blue Nile basin, Ethiopia.* ITC, Enschede. Retrieved from http://www.itc.nl/library/papers_2008/msc/wrem/wale.pdf

Ward, J. D., Werner, A. D., Nel, W. P., & Beecham, S. (2011). The influence of constrained fossil fuel emissions scenarios on climate and water resource projections. *Hydrology and Earth System Sciences, 15*(6), 1879-1893. doi: 10.5194/hess-15-1879-2011

Wilby, R.L., Dawson, C. W., & Barrow, E. M. (2002). SDSM – A Decision Support Tool for the Assessment of Regional Climate Change Impacts. *Environmental Modelling & Softwar, 17*, 147-159.

Wilby, R.L., Hassan, H., & Hanaki, K. (1998). Statistical Downscaling of Hydrometeorological Variables Using General Circulation Model Output. *Journal of Hydrology, 205*, 1-19.

Wilby, R. L., & Dawson, C. W. (2008). *SDSM 4.2 — A decision support tool for the assessment of regional climate change impacts*. Statistical DownScaling Model SDSM Version 4.2.

WMO. (2008). Regionalization of climate change information for impact assessment and adaptation from http://www.wmo.int/pages/publications/bulletin_en/archive/57_2_en/giorgi_en.html

Yang, Wei, Andreasson, Johan, Graham, Phil, L., . . . Fredrik. (2010). Distribution-based scaling to improve usability of regional climate model projections for hydrological climate change impacts studies. *Hydrology Research, 41*(3-4), 211-229.

APPENDIX A: DOUBLE MASS CURVE TO CHECK INCONSISTENCY

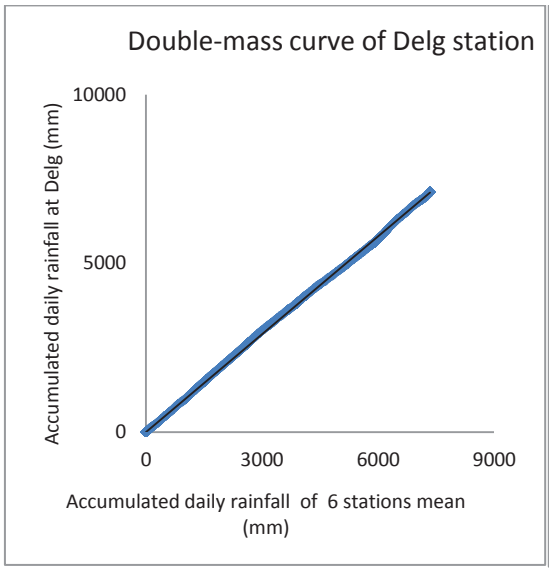

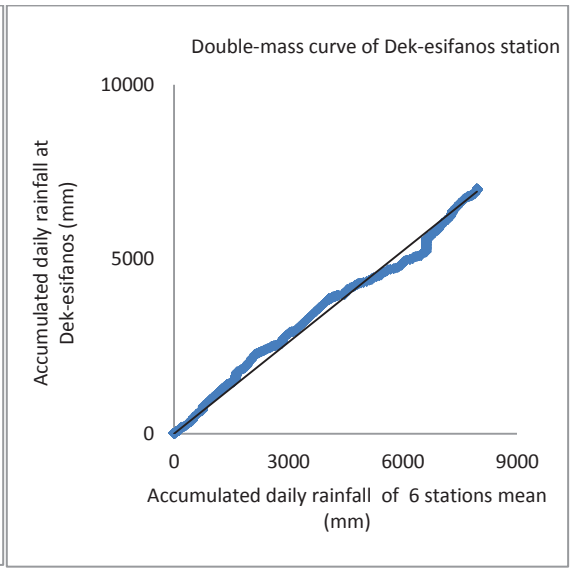

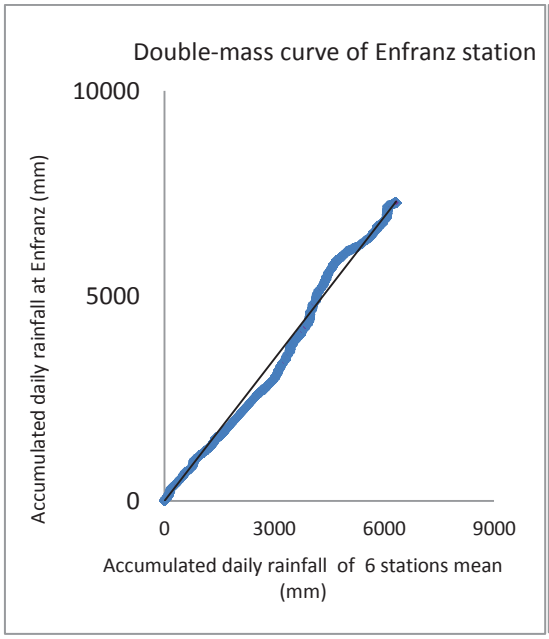

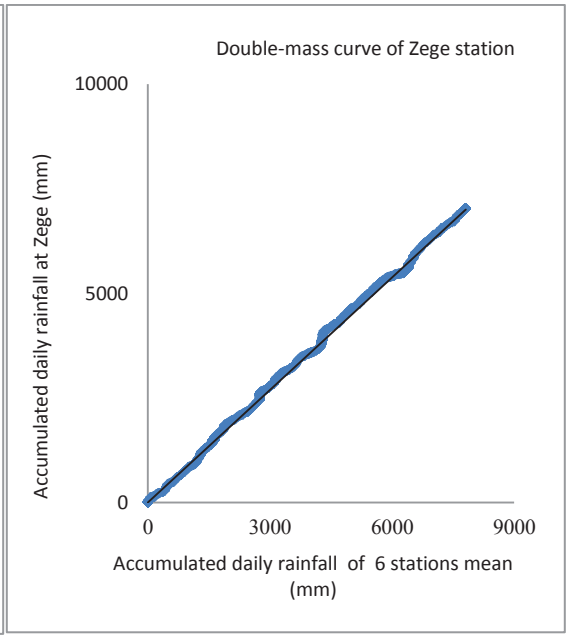

APPENDIX C: DEFINITIONS

Projection is common term in climate change literature with general and specific meaning. Generally, it refers any description of the future and the pathway leading while specifically the term refers "climate projection" to indicate model-derived of future climate.

Stastical significance is Statistical interpretation that indicates an occurrence was probably the result of a causative factor and not merely a chance result. Statistical significance at the 5% level indicates a 5 in 100 probability that a result can be ascribed to chance.

Normalization of NCEP predictors is calculating mean and standard deviation for the 1961-1990 period and subtracting the mean from each daily value before dividing by the standard deviation.

Partial correlation is the way of defining the unique relationship between the criterion and a predictor that represents the correlation between the predictor and given criterion after removing common variance with other predictors from both the criterion and the required predictor. After removing variance that the predictor and a criterion have in common with other predictors, the partial correlation expresses the correlation between the residualized criterion and the residualized predictor.

Normal precipitation is an average of the precipitation values over a 30-year period.

Baseline /Reference period is a time period against which change is measured. It defined as observed climate that usually combined with climate change information to develop a climate scenario; it serves as the reference period from which the modelled future change in climate is developed

The following definitions are taken from (IPCC,2007).

The A2 scenario refers a very heterogeneous world with causative theme of self-reliance and preservation of local identities. It characterized by continuously increasing population caused by very slowly converging fertility patterns across regions, regionally oriented and per capita economic growth lead economic development and more fragmented and slower technological changes than the other storylines.

The B2 scenario refers a heterogeneous world in which the emphasis is on local solutions to social, environmental and economic sustainability. It characterized by continuous increase of population at a rate lower than A2, intermediate level economic development with slow and more diverse technological change than the A1 and B1 storylines, and oriented toward social equity and environmental protection focusing on local and regional levels.

A1B is emission scenario with balanced dependence on all energy sources (i.e. by definition it is not relying too heavily on one individual energy source based on the assumption that similar enhancement rates apply to all energy supply and end use technologies). It characterized by fast economic growth and highest population in mid-century with a balance of non-fossil and fossil fuel demanding energy sources.

APPENDIX D: CATCHMENT EXTRACTION PROCEDURES (THIS WORK)

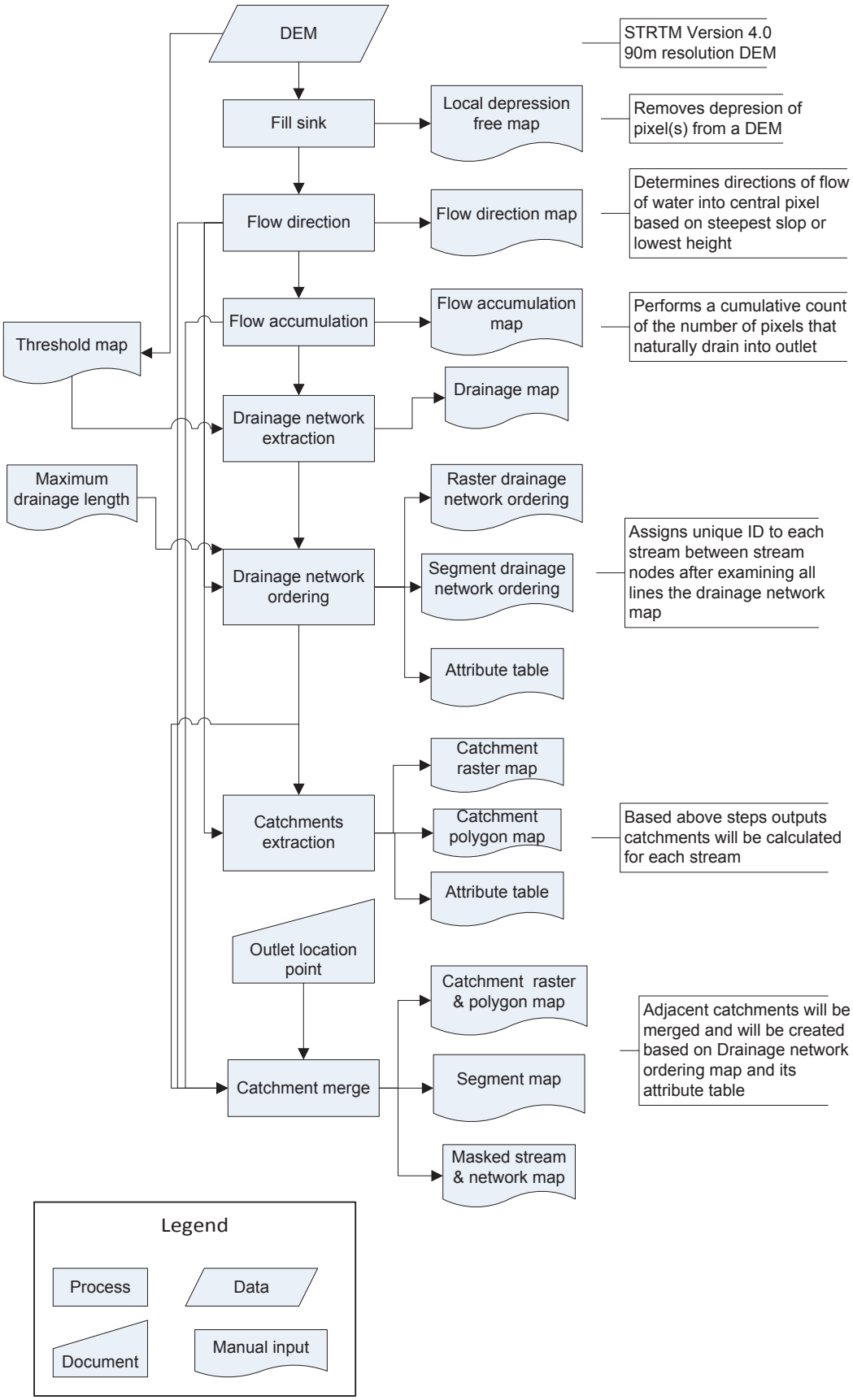

APPENDIX E: GENERAL PATTERNS OF SDSM AND RCM MODELS OUTPUT AT BAHIR DAR STATION

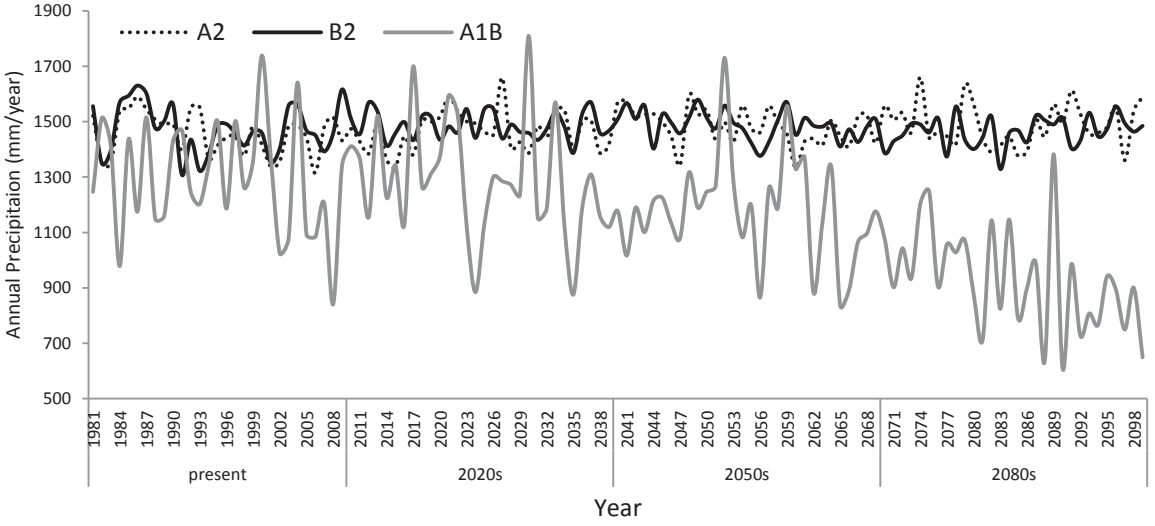

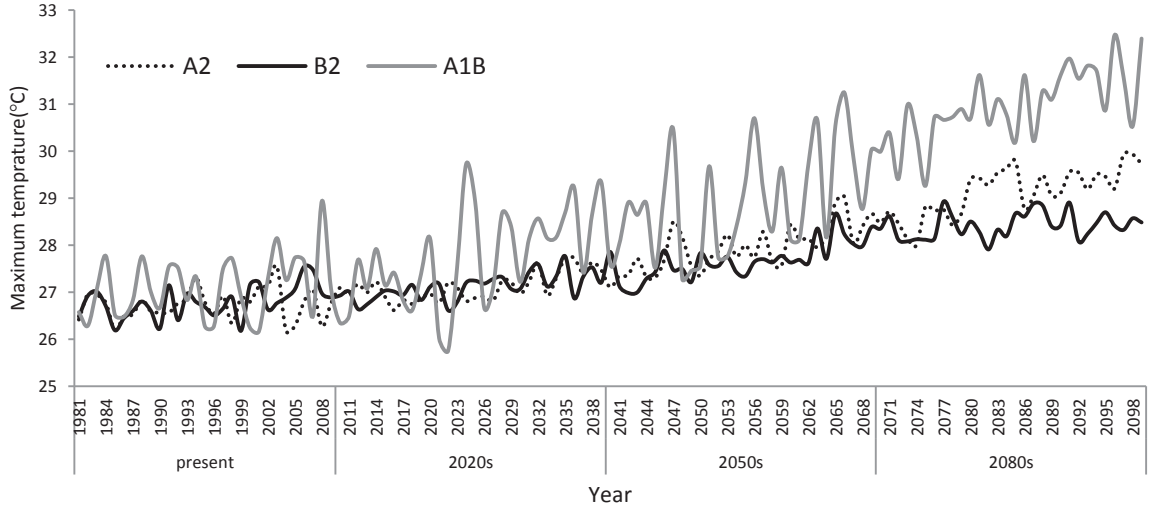

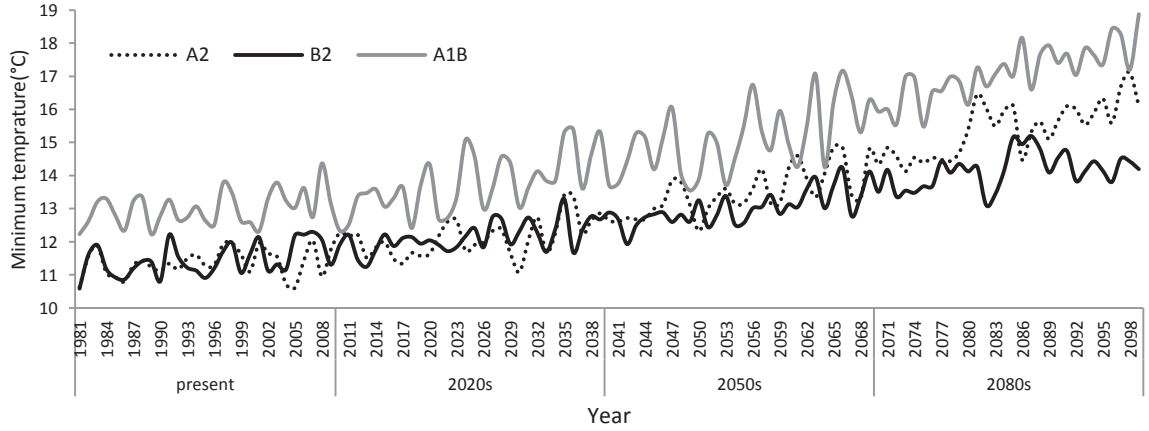

APPENDIX F: PHYSICAL CATCHMENT CHARACTERISTICS (PERERA,2009)

Gauged Catchments	Catchments area (km2) AREA	Longest flow path [km] LEP	DEM mean [m] MDEM	Hypsometric integral [-] HI	Average slope of catchment [%] AVGSLOP	Catchment shape [-] SHAPE	Circularity index [-] CI	Elongation ratio [-] EL	Forest [%] DD	Grass land [%] CROPD	Crop [%] CROPM	Bare land [%] GL	Woody savannah [%] URBAN	Build up area [%] FOREST	Leptosol area [%] LEP	Nitosol area [%] NIT	Vertisol area [%] VER	Luvisol area [%] luv	Standard annual average SAAR	Mean precipitation wet PWET	season (Oct. to May) PDRY	evapotranspiration [mm] PET
Ribb	1408	97.67	2915	0.48	44.59	61.73	38.49	1.55	444.38	51.53	30.66	12.79	0.06	4.96	38.58	0.3	0	36.84	1395	9.16	1.1	1300
Gilgal Abay	1657	81.58	2676	0.48	36.76	40.33	30.07	1.08	428.28	74.26	25.66	0	0.08	0	0	0.51	1.95	55.86	1750	10.61	1.84	1332
Gumera	1281	84.28	2717	0.48	33.68	53.36	34	1.5	420.27	64.27	31.34	3.86	0.08	0.45	9.23	0	3.27	87.21	1415	9.21	1.16	1307
Megech	531	43.92	2415	0.5	37.28	48.16	23.78	1.24	422.69	89.54	10.23	0.07	0.16	0	81.59	9.25	3.34	5.03	1117	7.09	1	1442
Koga	298	47.64	2429	0.43	23.48	70.16	46.68	1.75	397.48	69.61	24.25	0.03	0	6.11	4.11	7.69	14.67	47.61	1542	9.55	1.51	1349
Kelti	608	62.48	2229	0.46	20	31.24	33.48	1.39	431.05	99.99	0	0	0.01	0	0.2	0	8.25	91.55	1585	9.74	1.6	1305
Ungauged																						
Ribb	736	24.97	2264	0.46	24.91	31.15	40.55	1.36	461.27	73.71	16.06	8.74	0.02	1.47	9.86	0	13.37	23.94	1210	8.15	0.84	1311
Gilgal Abay	2072	79.96	2166	0.41	18.98	19.93	38.69	1.21	389.33	76.6	19.2	0.04	0.12	4.03	22.15	3.13	13.26	53.53	1486	9.86	1.12	1352
Gumera	287	17.87	1920	0.48	16.67	16.6	39.22	1.25	380	80.46	19.49	0.03	0.02	0	0	0	23	54.73	1368	9.13	0.98	1386
Megech	437	36.09	2234	0.46	18.04	46.75	37.2	1.75	457.42	97.91	2.06	0	0.03	0	18.88	0	47.66	13.69	1162	7.16	0.96	1359
Gumero	588	44.74	2230	0.47	27.87	46.55	30.49	1.03	395.47	71.85	28.14	0	0.01	0	48.65	3.65	35.17	10.58	1120	7.39	0.89	1340
Garno	463	37.64	2338	0.46	36.06	63.42	24.58	0.85	348.1	72.9	7.91	18.62	0.04	0.54	64.86	9.51	19.2	1.4	999	6.96	0.64	1498
Gelda	391	42.81	2093	0.47	17.95	34.42	35.42	1.27	355.9	60.73	38.93	0	0.33	0	0.46	0	1.44	97.52	1414	9.57	1.02	1498
Dema	325	45.87	2142	0.49	15.96	40.94	42.55	2.26	397.78	97.84	2.14	0	0.02	0	22.64	0	68.57	6.01	1131	7.04	0.87	1498
Tana west	546	12.81	2038	0.49	21.39	22.03	52.46	4.69	365.77	66.57	33.16	0	0.02	0.25	0	0	19.24	34.2	819	5.33	0.67	1444
Gabi Kura	427	26.21	2003	0.48	16.09	21.88	35.39	4.8	354.63	95.85	4.13	0	0.02	0	1.22	0	64.38	6.99	992	6.52	0.79	1498